Final work : Aeroelastic tailoring of carbon fiber blades

Auteur : Chalke, Akshay Prafulla
Promoteur(s) : Hillewaert, Koen
Faculté : Faculté des Sciences appliquées
Diplôme : Master en ingénieur civil en aérospatiale, à finalité spécialisée en "turbomachinery aeromechanics (THRUST)"
Année académique : 2020-2021
URI/URL : http://hdl.handle.net/2268.2/13073

THRUST Master of Science, 30 credits

KTH Royal Institute of Technology,
Stockholm, Sweden, 2021.

University of Liege,
Liege, Belgium, 2021.

Academic Year 2020-2021

Master Thesis Report

Aeroelastic tailoring of carbon fiber blades

Final work carried out with a view to obtaining the master's degree "Civil Engineer in Aerospace, specialized in turbomachinery aeromechanics (THRUST)" by Akshay Prafulla Chalke

Authors

Akshay Prafulla Chalke <akshaychalke39@gmail.com>/<chalke@kth.se>

School of Industrial Engineering and Management
KTH Royal Institute of Technology

Faculty of Applied Sciences
University of Liege

Supervisor

Nenad Glodic
Researcher, KTH Royal Institute of Technology
Mauricio Gutierrez Salas
Post Doc researcher, KTH Royal Institute of Technology
Koen Hillewaert
Professor, University of Liege

Abstract

In a quest to achieve lighter and more efficient turbomachines alternative materials like carbon fibre have emerged due to its light weight and anisotropic properties. The anisotropic nature has fuelled the curiosity to investigate if it can be used to enhance mechanical performance and provide aeroelastic stability where traditional titanium blades would fall short of requirements.

The current project aims to investigate the effects of using carbon fiber blades on the aeroelastic (flutter) stability of a first stage compressor rotor blade. In purview of the project a composite blade model is built in Ansys ACP following composite design guidelines. Steady aerodynamic analysis is performed at an off design point of interest and the obtained pressure loads are imposed in modal analysis to get modal results for the 1^{st} bending and 1^{st} torsion mode. The mode shapes are used in the flutter analysis to quantify aerodynamic damping which indicates the flutter stability.

A parametric study is conducted to investigate the effect of change in ply orientation on the static and modal properties and eventually aerodynamic damping of the blade. A set of cases are defined with different ply orientation and the stability is investigated for each case. It is found that increase in plies with orientation angle of 45° tends to increase stability of the blade for the 1^{st} bending mode. Also placement of more 45° plies towards the outer surface of the stackup provide higher stability. Overall a lower twisting and higher frequency is favourable for 1^{st} bending mode. This conclusion is not strongly observed for 1^{st} torsion mode. However, lower value of angles is observed to deviate the vibration behaviour from the classical first torsion mode and cause a shift in least stable nodal diameter to higher values. A stable stackup in one mode could be unstable in other thus the dependency on ply angle and arrangement of plies on aerodamping is observed to be complex and investigation in other ply angles and experimental validation is deemed necessary.

Acknowledgements

I would like to thank Mr. Nenad Glodic and Mr. Mauricio Salas for presenting me this opportunity to conduct my final research work at the HPT Lab in KTH Royal Institute of Technology. I also thank Professor Koen Hillewaert for being my supervisor from University of Liege. This thesis presented me challenges and helped me develop myself into learning and implementing methods to address design requirements. The guidance received from all of my supervisors helped me in fulfilling the requirements of the thesis work. Finally, I would like to thank my classmates from the THRUST program who helped me adapt to the new learning environment and equally contributed in my growth.

Acronyms

E	Young's modulus
E_l	longitudinal modulus
E_t	transverse modulus
E_M	modulus of matrix
E_F	modulus of fiber
G_M	shear modulus of matrix
G_F	shear modulus of fiber
V_M	volume fraction of matrix
V_F	volume fraction of fiber
p	fluid pressure
v	blade vibration velocity
n	blade surface normal
ND	nodal diameters
IBPA	interblade phase angle
FTW	Forward Travelling Wave
BTW	Backward Travelling Wave
δ	damping factor
ξ	damping ratio
s	scaling
ω	blade vibration frequency
W_{aero}	aerodynamic work per cycle
k	reduced frequency
f	blade vibration frequency
L_{ref}	reference length
U_{ref}	reference flow velocity

List of Figures

List of Tables

Contents

Chapter 1

Introduction

The necessity to reduce fuel consumption and improve power to weight ratio has led to the need of developing lighter and more efficient turbomachines. The use of carbon fiber material due to its high strength to weight ratio is seen as a potential alternative with carbon fiber already finding application in jet engine fan blades [14]. For any material used, the performance of aerospace structures like airplane wings or gas turbine blades is limited by the aeroelastic issues of which flutter is one of the dominant aeroelastic phenomena. Flutter is an unstable state occurring in structures subjected to aerodynamic, inertial and structural forces wherein the structure (eg: fan blade) undergoes self-excited vibration. These vibrations are a result of interaction between structural dynamics and the aerodynamic forces due to pressure fluctuations in the flow field. These pressure fluctuations are in turn influenced by the blade motion i.e the frequency and mode shape of the blade, and operating conditions[9]. These self excited vibrations can result in structural failure in very short period of time amounting to seconds. Thus it is very difficult to control it in operation and needs to be predicted well before its onset so as to avoid the critical region of flutter.

Besides providing the advantage of reduced weight, composite materials, which are composed of fibers held in a matrix, present properties dependent on the direction of fiber which is termed as anisotropy. The fibers are arranged in a ply, which are then stacked into laminates to form the composite structure. The property of the structure is influenced by the orientation of fibers in each ply [9]. Changing the orientation of plies in the laminate stackup thus provides a potential to change the mechanical properties of the stackup to desired requirements termed as tailoring. Thus the question here to

investigate is if this anisotropic properties can be tailored to achieve a static and modal response which can provide aeroelastic stability. Thus aeroelastic tailoring refers to adjusting the mechanical properties of the composite structure by changing the ply orientation to achieve aeroelastic stability.

Research investigating this is done in various works over the last decades and has shown the potential of tailoring composites to achieve stability. The most important works and their conclusion are presented in Section 1.1.

1.1 Background

Works by Kuang and Hsu [12] as early as 2002 have investigated the effects of parameters like ply orientation and internal damping on the natural frequencies of composite structures. The ply orientation, pre-twisted angle and rotation speed were found to have an effect on the eigenfrequencies, mode shapes and damping .

Investigations in potential of aeroelastic tailoring to improve flutter stability were made by Reiber et al. [9]. It showed a strong influence of stacking sequence on the structural and aeroelastic behaviour. From the modal analysis a strong dependence between longitudinal stiffness and reduced frequency and between torsional portion and shear stiffness was found. The authors established a relation between laminate properties and eigen behavior and between eigen behavior and aerodynamic stability. It was found that the combination of reduced frequency and torsional portion is decisive for aerodynamic stability. The authors analysed the structural behaviour of blade in software MSC Nastran and performed aerodynamic analysis with DLR CFD solver TRACE.

A method for design of composite compressor blades and a manufacturing method to produce prototypes for experimental evaluation was proposed by Wollman et al. [19]. The paper stated that the 0° layers carry the centrifugal load and provide a high bending stiffness. $\pm 45^\circ$ layers reduce the shear stress and the untwist of the blade. The 90° layer prevents the bend up of the blade profile. The paper also discussed the manufacturing feasibility and found Resin Transfer Moulding to be accurate up to 0.06 mm in thickness. Commercial software Abaqus was used for numerical analysis by authors.

A general ply lay-up and drop-off method for composite structure was summarized by

Xiao et al. [13]. The author highlights the importance of shuffling drop-off plies and also provides ply lay-up and ply drop-off criteria to avoid large stress concentration areas and other structural problems. The work involved numerical analysis of various stacking sequence to preform failure analysis by looking at the inverse reserve factor. The modal analysis results showed that with 0° and 45° plies most modes have high modal frequencies. 45° and 90° plies were found to enhance torsional stiffness. The possibility of 90° plies effecting higher order, bend dominating modes is concluded in the work. In case where pre-stress is considered -45° plies are expected to increase modal frequencies. Fibersim software was used by the authors to perform ply layup and then static and modal analysis was performed using Ansys.

A parametric study on dynamic analysis of composite laminated plate done by Ahmed [2] also emphasized the importance of ply orientation on the natural frequency of composite laminated plate. The other conclusions were that for the same plate thickness the natural frequency increases with number of plies up to 10 plies and also the frequency increase is almost doubled when the thickness is doubled.

Other works like by Bendiksen related to flutter suppression techniques [6] talked about increasing flutter and divergence speed by varying fiber orientation and ply stacking configuration. Tola et al. [10] in his works on subsonic and supersonic flutter in composite missile fin concluded that solely changing the sequence of the plies is enough for shifting the flutter speed to higher values without changing the weight and cost of the fin.

Experimental results by Mehmed [16] pertaining to classical flutter in composite turboprop model indicated a flutter frequency between first two blade normal modes. Tola et al. [10] also talks about flutter occurring due to coupling of first bending and first torsion modes which indicate them as the modes of interest.

All the above literature thus provides a promising hope into achieving flutter stability by changing ply orientations in composite blades. The use of commercial finite element tools is also found to provide acceptable results. This has motivated the current work to investigate tailoring of composite blade for a first stage compressor rotor. The effect of ply orientation for the current operating conditions is investigated and the previous works related to shuffling of plies and ply orientation angles are taken into consideration. The FEM modeling of the blade and aerodynamic stability investigations are done in Ansys 2019 R3.

1.2 Objectives

The thesis is aimed at implementing the research done in previous works to build a composite blade model for compressor rotor blades. It illustrates the methodology followed to build the blade in Ansys ACP following composite design guidelines. The setups to perform steady aerodynamic and unsteady flutter calculations to predict stability are elaborated. A set of cases for stacking sequence are investigated for the operating conditions critical for the project. The thesis aims at establishing the process and guidelines to develop a composite blade model which provides aeroelastic stability in critical regions of operation.

The objectives of the thesis are summarised as follows:

- To establish a methodology to built a composite blade model in Ansys ACP following composite design guidelines and shuffling of internal ply drops
- To built a setup to perform static, modal and aerodamping analysis in Ansys Workbench for composite blades
- To define cases with varying stackup configurations (varying stacking sequence) and investigate modal behaviour and aerodamping for each case.
- Establish relation between stacking sequence and terms in stiffness matrix and then between terms in stiffness matrix and modal properties and stability.
- Identify a stacking sequence providing stability for the current operating conditions

1.3 Methodology

In purview of the project a composite blade model is built in Ansys ACP following composite design guidelines prescribed in literature. Steady aerodynamic analysis is performed at an off design point of interest to obtain pressure loads. These pressure loads are then imposed on the composite blade and a rotation velocity is specified. A pre-stressed modal analysis accounting centrifugal and pressure loads is performed to obtain modal results for the first flexure mode (1F) and first torsion mode (1T). The mode shapes for these modes and extracted and imposed in a transient blade flutter simulation to quantify aerodynamic work on the blade. The aerodynamic work is

then scaled using the kinetic energy approach to find the aerodynamic damping factor. These values are used to access the stability of the system.

1.4 Stakeholders

The present thesis is done in coordination with the Heat and Power technology department at KTH Royal Institute of Technology. The thesis is part of the project conducted within the framework of the NFFP7 research project VIND (“ Virtual Integrated Demonstrator for Turbomachinery”)

1.5 Outline

Chapter 2 discusses the theoretical background about composites and flutter and the relevant theory to the current work. Chapter 3 will explain the construction of the FE model of the composite blade. Chapter 4 will elaborate on the Mechanical and aerodamping setup to calculate modal and aerodamping results. The investigated cases are also presented here. The tailoring of the composite blade will be addressed with a number of cases investigated for the flutter stability. The cases will represent stackups with different ply orientations. Chapter 5 presents and discusses the results in the project. Finally Chapter 6 will conclude with design rules for ply orientations and placement of the plies with respect to camber surface to achieve required results.

Chapter 2

Theoretical Background

In this chapter, a detailed description about theoretical background of composites and flutter phenomena is presented to elaborate the underlying physics leading to the investigations and conclusions of the thesis.

2.1 Composites

Composites by definition are materials formed by combination of two or more different materials. This provides composites with better properties than the individual constituents. A number of naturally occurring composites like wood which is formed by long cellulose fibers held together by lignin have inspired the current class of engineering composites.

The structural composition of composites is illustrated in figure 2.1.1. At microscopic level composites consist of fibers and matrix as the base constituents which are arranged and homogenized into a ply which is the meso or macroscopic level. The fibers act as the load bearing member while the matrix transmits the load to the fibers and holds them in the desired arrangement. The individual plies are then assembled on each other to form the laminate which is at the macroscopic level. The plies can be stacked upon each other with the fiber orientation in each ply being at a different angle to the structural axis (1,2,3). The arrangement of the plies with varying fiber orientation forms a stacking sequence. The stacking sequence and its designations will be discussed in detail later in the chapter.

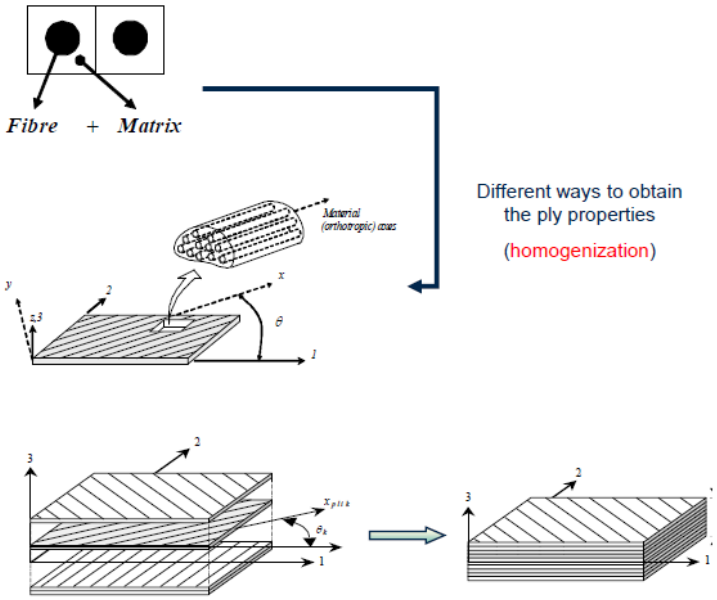

Figure 2.1.1: Composition of a composite structure from microscopic to macroscopic level. The fibres and matrix form the microscopic level which when homogenised together form the ply at the mesoscopic level. The plies are stacked together at varying fiber orientation with respect to the structural axis (1,2,3) to form the laminate. [8]

The fibers and the matrix play an important role as the properties of the laminate are derived from the properties of fibers and matrix, their volume fractions, and the arrangement of fibers. The properties at ply level are given by the laws of mixture by the relations 2.1 to 2.5. It is to be noted that these ply level properties are in direction of the orthotropic (fiber) axis. The orthotropic axis (ply level) (x,y,z) and the structural axis (laminate level) (1,2,3) are illustrated in figure 2.1.2

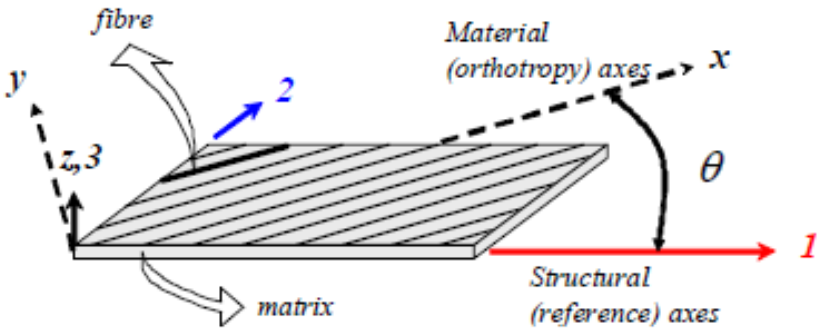

Figure 2.1.2: The orthotropic or material axis (x,y,z) is in the fiber direction and structural axis (1,2,3) in global direction [8]

The Young's modulus (E) in the orthotropic X-direction is the longitudinal modulus (E_l) and in the orthotropic Y-direction is the transverse modulus (E_t). The modulus of matrix (E_M), modulus of fiber (E_F), volume fraction of matrix (V_M) and volume fraction of fiber (V_F) form the equation 2.1 and 2.2 for E_l and E_t.

$$E_x = E_l = E_M.V_M + E_F.V_F \tag{2.1}$$

$$E_y = E_t = E_M \left[\frac{1}{(1 - V_F) + \frac{E_M}{E_F}.V_F} \right] \tag{2.2}$$

The Poisson ratio of matrix (ν_M) and fiber (ν_F) together with the volume fractions V_M and V_F give the Poisson's ratio of ply in xy direction in equation 2.3. Similarly the shear modulus of matrix (G_M) and shear modulus of fiber (G_F) together with the V_M and V_F give the shear modulus in xy direction in equation 2.4

$$\nu_{xy} = \nu_{lt} = \nu_M.V_M + \nu_F.V_F \tag{2.3}$$

$$G_{xy} = G_{lt} = G_M \left[\frac{1}{(1 - V_F) + \frac{G_M}{G_F}.V_F} \right] \tag{2.4}$$

$$\nu_{yx} = E_y.\frac{\nu_{xy}}{E_x} \tag{2.5}$$

The stiffness matrix of a ply in the orthotropic (fiber) axis is given by equation 2.6

$$Q_{(x,y,z)} = \begin{bmatrix} mE_x & m\nu_{yx}E_x & 0 \\ m\nu_{xy}E_y & mE_y & 0 \\ 0 & 0 & G_{xy} \end{bmatrix} = \begin{bmatrix} Q_{xx} & Q_{xy} & 0 \\ Q_{yx} & Q_{yy} & 0 \\ 0 & 0 & Q_{ss} \end{bmatrix} \tag{2.6}$$

where, m = $\frac{1}{1-\nu_{xy}\nu_{yx}}$

The stiffness matrix in the structural axis of a ply with fibers oriented at an angle θ with

the structural axis is given by equation 2.7

$$Q(\theta)_{(1,2,3)} = \begin{bmatrix} Q_{11} \\ Q_{22} \\ Q_{12} \\ Q_{66} \\ Q_{16} \\ Q_{26} \end{bmatrix}_{(1,2,3)} = \begin{bmatrix} c^4 & s^4 & 2c^2s^2 & 4c^2s^2 \\ s^4 & c^4 & 2c^2s^2 & 4c^2s^2 \\ c^2s^2 & c^2s^2 & c^4+s^4 & -4c^2s^2 \\ c^2s^2 & c^2s^2 & -2c^2s^2 & (c^2-s^2)^2 \\ c^3s & -cs^3 & cs^3-c^3s & 2(cs^3-c^3s) \\ cs^3 & -c^3s & c^3s-cs^3 & 2(c^3s-cs^3) \end{bmatrix} \begin{bmatrix} Q_{xx} \\ Q_{yy} \\ Q_{xy} \\ Q_{ss} \end{bmatrix}_{(x,y,z)} \tag{2.7}$$

where,

c = cosine(θ)

s = sine(θ)

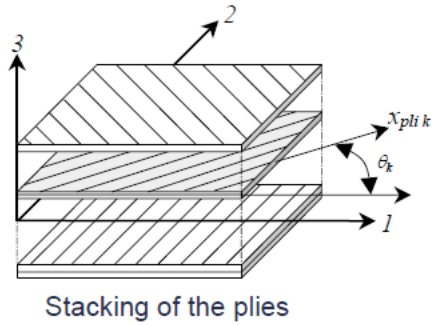

Stacking of the plies

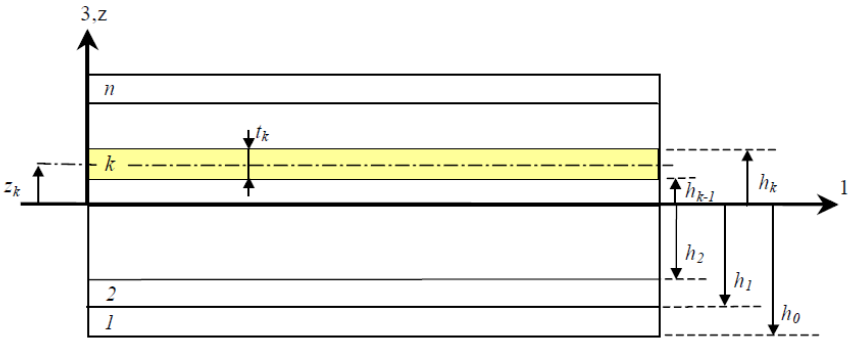

Figure 2.1.3: Stacking of plies into laminates with t the thickness of plies and h the distance of the ply from the symmetry axis [8]

At laminate level a number of such plies are stacked together at varying fiber orientations with the structural axis as shown in figure 2.1.3. The resulting stiffness matrix of the laminate is derived from the kinematics of Kirchoff's plate which gives the

relation of the loads and moments to the strains and curvature through the stiffness matrix of laminate. The relation is given as in equation 2.8

$$\begin{bmatrix} N_1 \\ N_2 \\ N_6 \\ M_1 \\ M_2 \\ M_6 \end{bmatrix} = \begin{bmatrix} A_{11} & A_{12} & A_{16} & B_{11} & B_{12} & B_{16} \\ A_{12} & A_{22} & A_{26} & B_{12} & B_{22} & B_{26} \\ A_{16} & A_{26} & A_{66} & B_{16} & B_{26} & B_{66} \\ B_{11} & B_{12} & B_{16} & D_{11} & D_{12} & D_{16} \\ B_{12} & B_{22} & B_{26} & D_{12} & D_{22} & D_{26} \\ B_{16} & B_{26} & B_{66} & D_{16} & D_{26} & D_{66} \end{bmatrix} \begin{bmatrix} \epsilon_1^0 \\ \epsilon_2^0 \\ \epsilon_6^0 \\ \kappa_1^0 \\ \kappa_2^0 \\ \kappa_6^0 \end{bmatrix} \tag{2.8}$$

The stiffness terms of the laminate are derived from the contribution of stiffness terms of the each individual ply and the thickness and position of each ply from the symmetry axis. The relations are presented in Equation 2.9, 2.10, 2.11

$$A_{ij} = \sum_{k=1}^{n} [Q_{ij}(\theta_k)](h_k - h_{k-1}) \tag{2.9}$$

$$B_{ij} = \frac{1}{2} \sum_{k=1}^{n} [Q_{ij}(\theta_k)](h_k^2 - h_{k-1}^2) \tag{2.10}$$

$$D_{ij} = \frac{1}{3} \sum_{k=1}^{n} [Q_{ij}(\theta_k)](h_k^3 - h_{k-1}^3) \tag{2.11}$$

Thus, it can be observed that the stiffness matrix of the laminate is dependent on the stiffness matrix of each ply given in the structural axis, thickness of ply and the position of ply from the symmetry plane. This highlights the dependency of the laminate stiffness matrix on the fiber orientation θ_k of the each ply (k) . This dependency can be exploited by changing the orientation of fibers in the plies and thus tailoring the stiffness properties of the laminate so as to achieve desired structural behaviour. The terms A_{ij} in the stiffness matrix denote the in-plane stiffness terms while the terms D_{ij} denote the out-of plane stiffness terms. The terms B_{ij} represent the coupling between the in-plane and out-of plane stiffness terms.

A laminate stackup as shown in figure 2.1.3 has a number of plies above and below the center line and each ply has a specific angle of the fiber orientation. The designation of the laminate stackup is given as follows:

$$[\theta_1 m_1 b_1 / \theta_2 m_2 b_2]_{nsb}$$

where

θ_1, θ_2 = ply orientation in the laminate

m_1,m_2 = number of plies of each particular orientation θ_1, θ_2. not used for a single ply with that orientation

b_1,b_2 = material type and form

n = number of repetitions of group

s = indication of geometric symmetry

A stacking sequence [15/-15/0/15/-15/15/-15/0/15/-15/-15/15/0/-15/15/-15/15/0/-15/15] can be written in condensed form as [(±15/0/±15)2]s. An example of designating a stackup is provided in figure 2.1.4

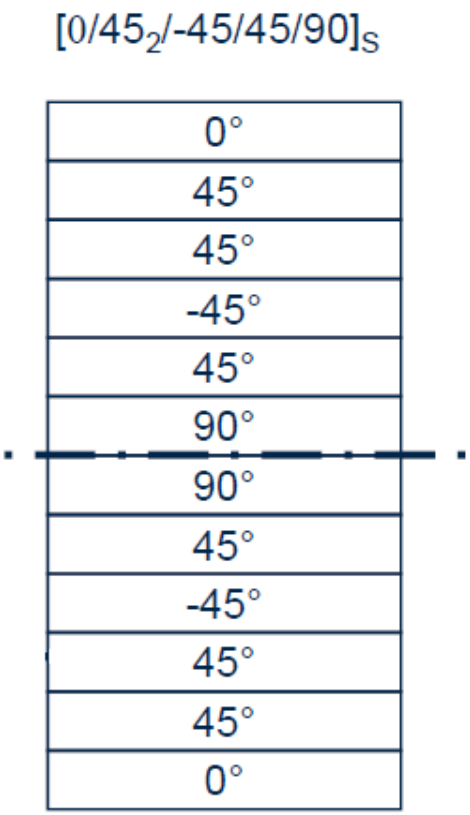

Figure 2.1.4: Example of stackup nomenclature [8]

2.2 Aeroelastic phenomena: Flutter

Aeroelasticity is a branch of engineering which deals with the interaction of inertial, structural and aerodynamic forces on structures like aircrafts, turbomachinery blades, buildings etc. The triangle as shown in figure 2.2.1 linking all this different sources of influence was given by Collar [11] and is termed as the Collar's triangle.

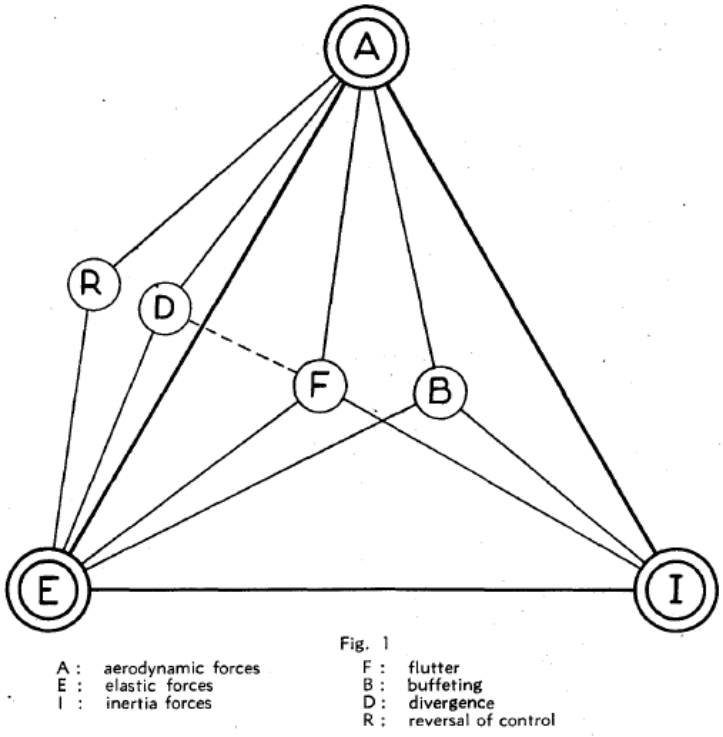

Figure 2.2.1: Collar's triangle linking the various sources of interactions leading to aeroelastic phenomena [11]

The domain of aeroelasticity can be further divided based on which forces interact. The interaction between structural or elastic (E) and inertial (I) forces is termed as structural dynamics. The interaction between inertial and aerodynamic (A) forces gives flight dynamics and finally the interaction between aerodynamics and structural forces gives static aeroelasticity (eg:divergence). The phenomena involving the interaction of all the the three forces is termed as dynamic aeroelasticity (eg: flutter).

Flutter in turbomachines is an unstable state wherein the blades undergo self-excited vibration with increasing amplitude until failure. In a turbomachine a number of blades are arranged around the circumference of disk forming each stage of the compressor or turbine. The motion of each blade is responsible for a perturbation in

the flow field causing pressure fluctuations around it which in-turn induces a response on that blade as well as the adjacent blades. This response is not only restricted to the immediate neighbouring blades but also affects a number of adjacent blades in the row. This phenomenon is termed as aerodynamic coupling and is the driving factor in occurrence of flutter.

The flutter phenomena can be mathematically understood from the general equations of motion from structural dynamics given in equation 2.12. The aerodynamic forces $\vec{F}_{aero}$ is composed of external force $\vec{F}_{ext}$ coming from the adjacent rows and forces due to coupling of the blades $\vec{F}_{coupled}$. The coupled forces can be further decomposed into velocity and displacement dependent terms C_{aero} and K_{aero} respectively and added to the left hand side of the equation. The new terms C_{aero} and K_{aero} are termed as the aerodynamic damping and aerodynamic stiffness terms as in equation 2.14.

$$M_s\ddot{x} + C_s\dot{x} + K_s x = \vec{F}_{aero} \tag{2.12}$$

$$M_s\ddot{x} + C_s\dot{x} + K_s x = \vec{F}_{ext} + \vec{F}_{coupled} \tag{2.13}$$

$$M_s\ddot{x} + (C_s + C_{aero})\dot{x} + (K_s + K_{aero})x = \vec{F}_{ext} \tag{2.14}$$

It was proven by Srinivasan [4] that the material damping of aeroengine blade is very small and the main damping comes from the aerodynamic one. Thus the total damping of the system is almost equal to the aerodynamic damping in absence of friction. Thus aerodynamic damping is a major variable determining the stability of aeroelastic system for flutter.

In commercial softwares like Ansys aerodynamic damping is determined from the aerodynamic work performed by the blade per cycle of vibration. Aerodynamic work is a measure of the exchange of energy between the blade and flow. Aerodynamic work per cycle (W_{cycle}) as calculated in Ansys CFX [3] is given by equation 2.15. This work is given by the product of the fluid pressure (p) and blade vibration velocity (v) in blade surface normal (n) direction integrated over the area of the blade and over time period of one oscillation. As per convention in Ansys a positive aerodynamic work indicates a transfer of energy from the blade to the flow thus indicating a damped vibration, while a

negative work indicates addition of energy to the blade thus leading to instability.

$$W_{Cycle} = \int_{t_0}^{t_0+T} \int_A p\vec{v}.\hat{n}\, dA dt \tag{2.15}$$

The fluid pressure and vibration of blade which determine the work per cycle are governed by various factors as highlighted in the Ishikawa diagram for flutter stability [17] in figure 2.2.2.

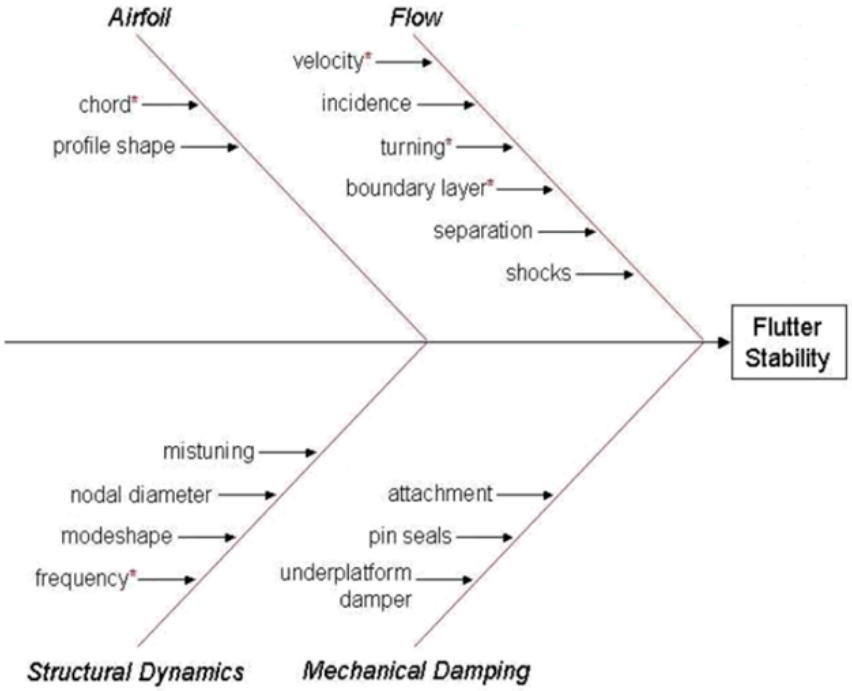

Figure 2.2.2: Ishikawa factors influencing flutter stability [17]

As from figure 2.2.2 the aerodynamic work is influenced by airfoil, flow, structural dynamics and mechanical damping. In the present thesis work the airfoil and the flow factors are fixed by design and operating requirements while the mechanical factors are difficult to model and quantify due to complexity of contact phenomena. The mechanical factors have a stabilizing effect in terms of flutter hence can be neglected as conservative approach. Thus the only factors that remains free variables are related to the structural dynamics.

This current work aims to investigate the effects of changing these structural dynamics variables to achieve flutter stability.

2.3 Structural dynamics of Bladed disks

A turbomachine consists of one or several stages with each stage consisting of stator and a rotor blade rows. Typically, each row is a disk with blades mounted on the circumference of the disk. Thus, it is important to consider the the dynamics involved both due to the blade and the disk. The blades under the assumption of being perfectly fixed to the hub and the disk being stiff exhibit classical beam bending modes. In context of blades the modes are referred to the direction of principle axis and are the flap mode/bending mode perpendicular to the chord, the edgewise bending mode parallel to the chord and the torsion mode about the radial axis. Representation of the three basic natural modes is shown in figure 2.3.1 with the red color highlighting the maximum displacement and the blue color the minimum. Further modes appear as a combination of these three basic modes with one or multiple inflexion points with zero modal displacement [20].

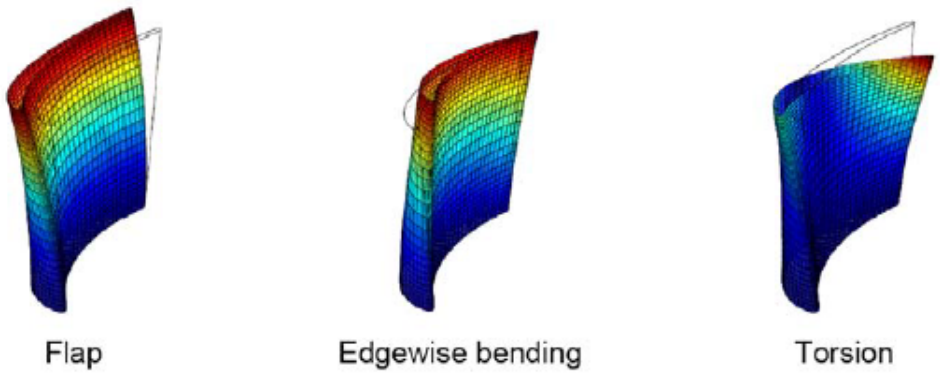

Figure 2.3.1: Basic natural mode shapes of blades [20]

The disk of turbomachine in its simplified form resembles a circular flat plate with axial, radial and tangential modes. The axial mode is the one mostly encountered and as seen in figure 2.3.2 is a combination of positive (out of page) and negative (in page) displacements separated by lines with no displacement. These lines are termed as nodal diameters (ND). An increase in ND increases the stiffness and thus the natural frequency of the disk.

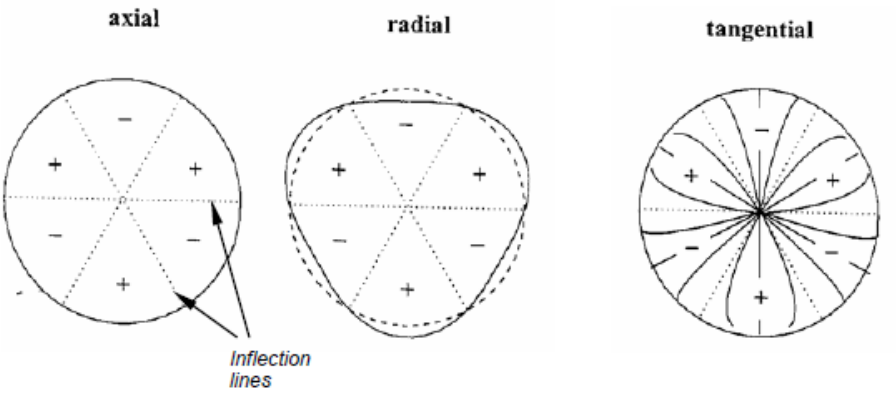

Figure 2.3.2: Basic natural mode shapes of disk [20]

A blade row is a combination of blade and a disk and the vibration behaviour is influenced by the their relative stiffness. A stiff disk and flexible blades exhibits a blade dominated vibration behaviour while a flexible disk and stiff blades exhibit a disk dominated behaviour. The blade and disk dominated modes can be observed in the frequency vs ND plot in figure 2.3.3.

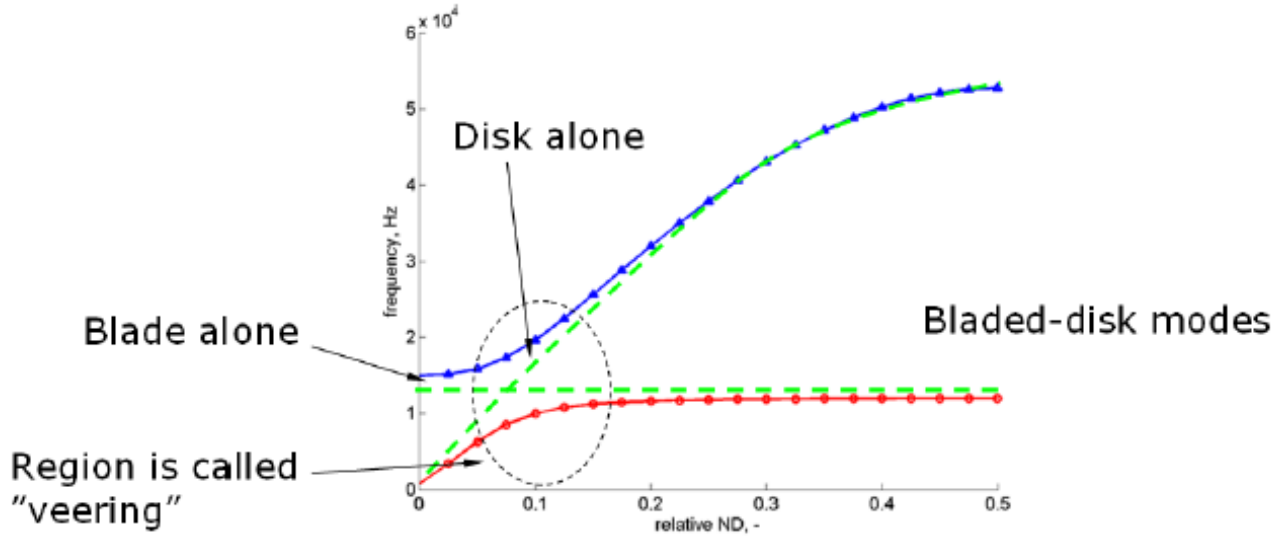

Figure 2.3.3: Blade and disk dominated modes showed in reference to the Nodal diameters [20]

The red line indicates the blade dominated modes which are fairly constant over the large range of ND. The disk dominated modes shown in blue show a higher frequency for higher ND. There is also a potential zone called the veering zone which represent an interaction between the blade and disk dominated modes where at low ND the

blade modes are disk dominated and the disk modes are blade dominated. The flutter phenomena is susceptible at any of the ND hence each ND is required to be investigated for the possibility of occurrence of flutter.

In a bladed disk the maximum possible number of ND that can be distinguished depends on the number of blades on the disk. For a blisk with even number of blades the maximum number of ND is given by equation 2.16 and for odd number of blades is given by equation 2.17

$$ND = \pm\frac{N}{2} \tag{2.16}$$

$$ND = \pm\frac{(N-1)}{2} \tag{2.17}$$

These ND are responsible for the phase difference between the vibration of adjacent blades vibrating at same amplitude as found by Lane [15] . This phase difference is termed as interblade phase angle (IBPA) and is applicable to a tuned system. A tuned system is one in which the manufacturing variations in the blade structural characteristics are not accounted and all the blades are assumed to behave identically. The IBPA results in a travelling wave pattern as shown in figure 2.3.4. The travelling wave is divided into Forward Travelling Wave (FTW) and Backward Travelling Wave (BTW) and given by equation 2.18 and 2.19.

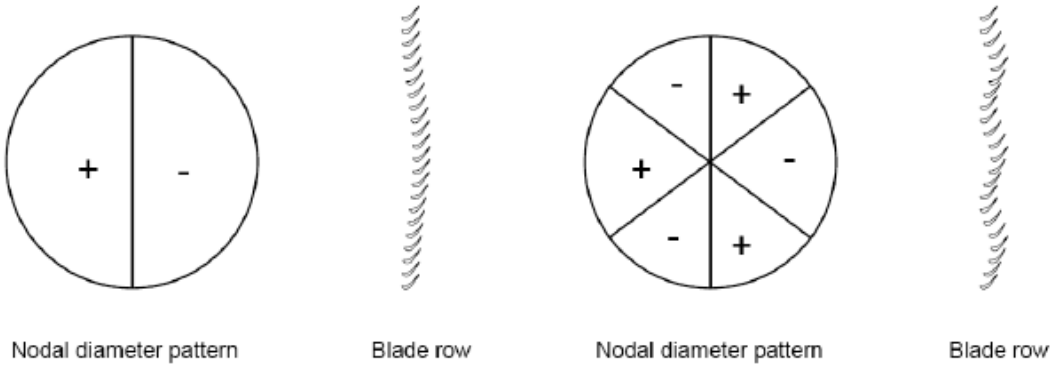

Figure 2.3.4: Travelling wave patterns for different ND [20]

$$FTW, \sigma = \frac{(2\pi ND)}{N} \tag{2.18}$$

$$BTW, \sigma = 2\pi \frac{(N - ND)}{N} \tag{2.19}$$

Thus each nodal diameter for a forward and backward travelling wave behaviour is a potential point of flutter instability. Thus each of this point is to be investigated to find the least stable point.

Along with the mode shape and nodal diameters described above the frequency of vibration is also a decisive structural dynamic factor. The frequency is generally expressed as the reduced frequency and is given by equation 2.20, where reduced frequency (k) is the multiple of blade vibration frequency (f) in [Hz] and reference length (L_{ref}) divided by the reference flow velocity (U_{ref}). The L_{ref} is half chord length and the U_{ref} is the mass flow averaged velocity at the domain inlet. According to Brouillet [5], the limits on reduced frequency for flutter stable behaviour are k>0.3 for bending mode and k>0.7 for torsional mode.

$$K = \frac{2\pi f L_{ref}}{U_{ref}} \tag{2.20}$$

2.4 Chapter conclusion

Composites due to its anisotropic properties provide an opportunity to modify the structural variables like mode shape and frequency without affecting the shape of the blade. As elaborated in the Section 1.1 these variables can be influenced by orientation of the ply, thickness of the ply and its position from the symmetry axis. The thickness of the ply being a variable depending on manufacturers catalogue will be fixed while the orientation and position will be changed to study the effects. These mode shapes and frequency changes are a part of the structural dynamic factors which affect aerodynamic damping and thus the flutter stability of the system. For each mode there exist a number of nodal diameters that can be excited and need to be investigated for flutter stability. Thus the task carried out further is to investigate the effect of the composite stackup on the mode shape and frequency of a particular mode and the corresponding effect on flutter stability for each nodal diameter for that mode.

Chapter 3

Building FE model of composite blade

A key to a good study and reliable analysis is a good numerical model. It is important that the the numerical model built should accurately represents the physics and the results should be independent of the numerical parameters. The procedure to build the model is elaborated in section 3.1 and its check for reliability of results is presented in the section 5.1

3.1 Procedure to build the model

Commercial software Ansys ACP is used for building the numerical finite element model of the composite blade. Ansys ACP provides features which help the user to define plies and build stackups as they would be done in actual manufacturing scenario. Previous work by Xiao et al. [13] have used Fibersim while Reiber et al. [9] have used MSC Nastran to build the composite blade model. An attempt is made to use Ansys ACP for the current project and the procedure is illustrated below. Previous works show that the composite blade model can be built using two approaches namely the onion skin configuration as followed by Xiao et al. [13] and the blade milling approach used by Forsthofer et al. [18]. In the former the plies are initially cut to a specific shape and laid over each other to form the final shape of the structure. In the latter flat plates, pressed from thermoplastic fibers, called as organosheets are stacked parallel to each other and then milled to obtain the complex blade shape. This method is a demonstrator technology in which the conventional composite design rules are violated. Extensive

testing to ensure integrity of the structure is required to be performed for the latter approach. In the current work the onion skin configuration is followed to abide by the composite design rules. The rules as described by Xiao et al. [13] are listed down below:

Ply drop criteria:

1. Covering
   The upper and lower surface of the whole structure should not be designed as a ply drop layer
2. Maximum Taper Slope
   The taper angle should not exceed 7°. i.e the length of the decreasing portion should be at least 8 times the length of ply thickness
3. Maximum Ply drop number
   The number of ply drop layers of same height should not exceed 2 at one position
4. Internal continuity
   Continuous plies should be kept in between dropped plies
5. Alternating
   The ply-drop layers should be as scattered as possible.

Ply Layup criteria:

1. Symmetry
   Ply layup should be symmetric around the midplane
2. Balance
   The stacking sequence should have equal $+\theta$ and $-\theta$ layers
3. Proximity principle
   No more than a given number of plies of same orientation should be stacked together. The number is set to 4 here.
4. Disorientation
   The maximum difference in orientation of adjacent plies shouldn't exceed 45°
5. 10% rule
   The number of plies of a particular orientation should not be less than 10 % of total ply numbers.

6. Surface ply angle

   The upper and lower surface of the entire structure should not be a 0° ply

The blade geometry under investigation is placed in figure 3.1.1a

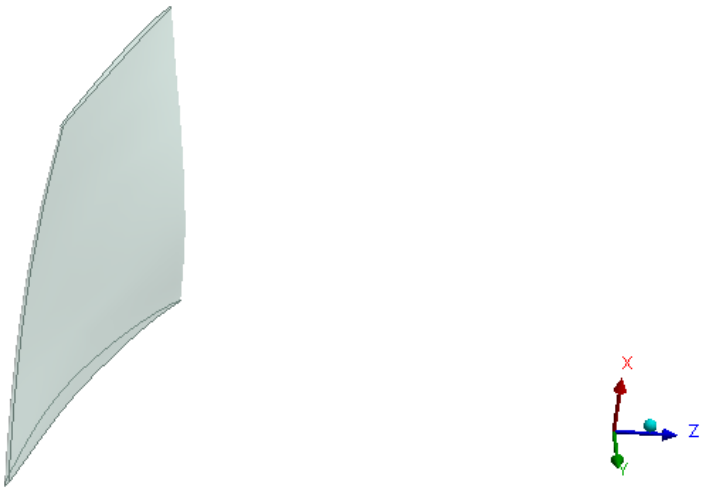

(a) Geometry of solid blade

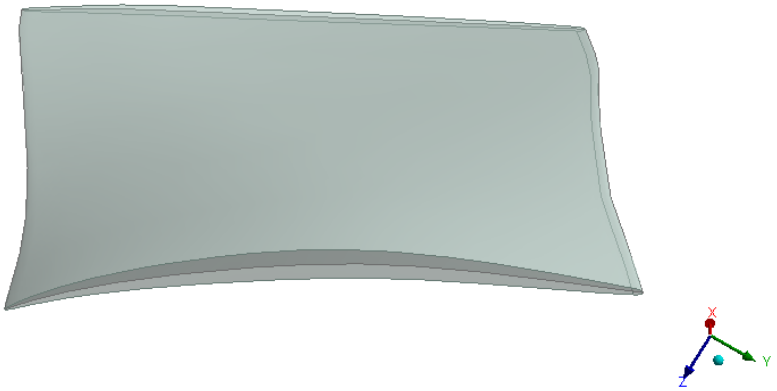

(b) Surface of blade suction and pressure face serving as the limiting geometry and the camberline surface in between serving as the starting geometry

Figure 3.1.1: Blade solid geometry and surface geometries used for creation of composite blade model

The geometric details of the blade are placed in table 3.1.1

Parameter	Value	Units
Blade chord	0.10761	[m]
Span at leading edge	0.1561	[m]
Span at trailing edge	0.12874	[m]

Table 3.1.1: Details of blade geometry

To build blade model in Ansys ACP it is required to define a starting surface on which the ply definitions i.e the ply with a particular fiber orientation will be specified. Also surfaces defining the limits to the plies are required so as to obtain the desired blade shape. The camberline surface extracted serves as a base geometry for the ACP module on which the composite plies are laid in both directions to form the final blade model. The pressure and suction surfaces extracted serve the purpose of defining the limiting surfaces up to which the plies are laid up.

The first task in the composite blade construction is the specification of material to be used. The material definitions used by Xiao et al.[13] are available in the Ansys material library and are used for the current project. The properties of the fabric in orthotropic axis are mentioned in the table 3.1.2. The ply thickness used is 0.125 mm. Epoxy resin is used as a binding material and drop off material in the blade construction. The properties are mentioned in table 3.1.3

Parameter	Value	Units
Fabric designation	Epoxy carbon UD (230 GPa) Prepreg	[-]
Density	1490	[kg/m3]
Young's modulus in x (fiber) direction	121	[GPa]
Young's modulus in y and z direction	8.6	[GPa]
Shear modulus in xy and xz direction	4.7	[GPa]
Shear modulus in yz direction	3.1	[GPa]
Tensile Stress Limit in x Direction	2231	[MPa]
Tensile Stress Limit in y and z Direction	29	[MPa]
Compressive Stress Limit in x Direction	-1082	[MPa]
Compressive Stress Limit in y and z Direction	-100	[MPa]
Shear Stress Limit in xy and xz Direction	60	[MPa]
Shear Stress Limit in yz Direction	32	[MPa]
Poisson's ratio in xy and xz Direction	0.27	[-]
Poisson's ratio in yz direction	0.4	[-]

Table 3.1.2: Material properties of composite fabric used for composite blade

Parameter	Value	Units
Resin designation	Resin Epoxy	[-]
Density	1160	[kg/m3]
Young's modulus	3780	[GPa]
Shear modulus	1400	[GPa]
Poisson's ratio	0.35	[-]

Table 3.1.3: Material properties of resin used for composite blade

After defining the materials in engineering data the geometry module is imported in workbench and the camber surface is imported in the design modeler. The thin command is applied to keep surface with zero thickness. The camber surface in design modeler can be seen in figure 3.1.2a

The camber surface and the engineering data is then imported into the ACP-pre module. In the ACP-pre Mechanical module the material and an arbitrary thickness is assigned to the surface body. A quadratic mapped face mesh with all quadrilaterals is defined on the surface. The element size used in the project is 3 mm(186918 Nodes) which is later justified in mesh independence study in section 5.1. The mesh defeaturing is enabled and curvature and proximity capture is disabled. Named selection for the leading and trailing edge are defined in this section. The surface mesh can be seen in figure 3.1.2b

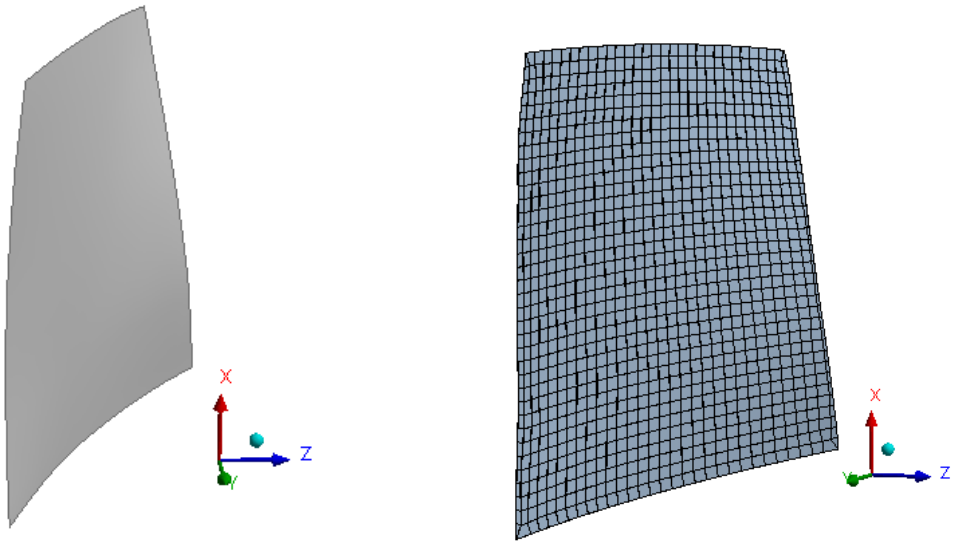

(a) Camber surface used in ACP module

(b) Surface Mesh on camber surface

Figure 3.1.2: Camber surface and the surface mesh on the camber surface used as a starting reference on which the ply layup definitions are built

Once meshed, the ACP-pre setup module is used to specify layup definitions. The pictorial illustration of the process is presented in figure 3.1.3 and described below. The fabric and resin material data is directly imported from the engineering data. The fabric is then created with a thickness of 0.125 mm and cut-off and drop-off material options set to the epoxy resin. The elements sets and edge sets are left to the default option. A entity named rosette is available in ACP which serves the purpose to define

the fiber direction. One such rosette is then created, the x-axis of which is directed in the radial direction towards the bade tip and it specifies the 0° fiber orientation. Another entity named oriented selection set is used to define the direction of ply layup. The rosette is specified in the oriented selection sets where the direction of fiber is referenced to the direction of rosette. Two oriented selection sets (red:pressure side and blue:suction side) define the direction for the stackups in two opposite direction from the camber surface (green). This specifies ACP to layup plies on both side of the camber surface. Next a geometry definition (red:pressure side surface and blue:suction side surface) is provided to specify the limits to the ply lengths so as to adopt to the blade shape. These limits are specified through the cut-off selection rules which are applied to each ply. This rule leads to the plies being cut at the intersection with the geometry. The reference geometry and the offset from the geometry are inputs for the cut-off selection rules. The cut-off selection rule and its use for the shuffling of ply drops will be discussed in detail later in this chapter. Then the modeling groups are created for the suction and pressure side and 25 plies are defined in each modelling group. The oriented selection sets and fiber direction are specified in the ply definitions. Here, the sign of the fiber angle for pressure and suction side should be opposite to have a symmetric stackup. The oriented selection sets provide the direction of layup for the modeling groups. The most important parameter defining the shape of the blade which is the cut-off selection rule is specified in the ply definitions. Finally the solid model is created which builds the model in accordance to the ply definitions.

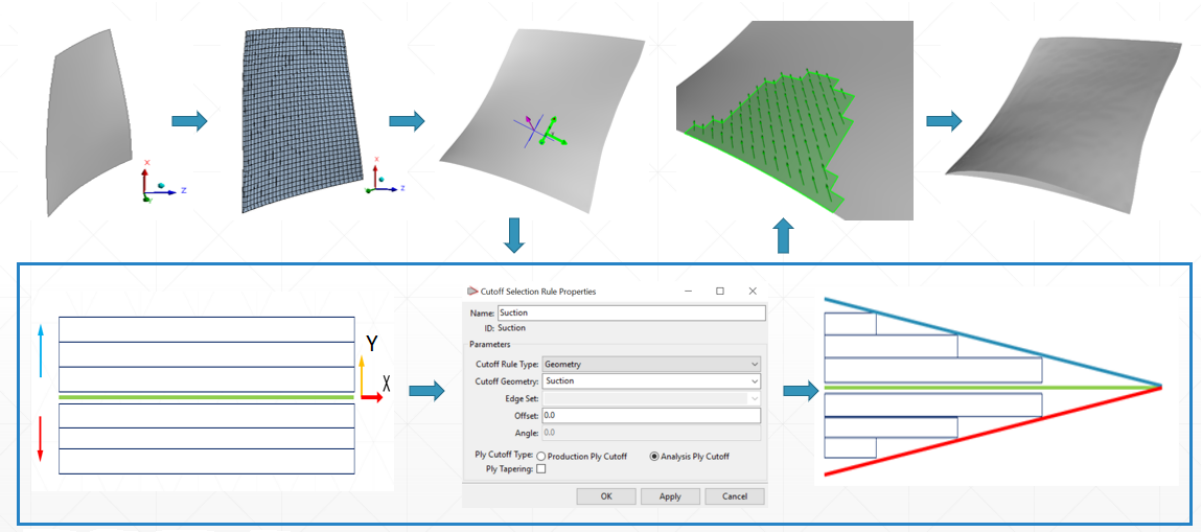

Figure 3.1.3: Process of building a composite blade model starting from camber surface > surface mesh > rosette and oriented selection set > cut off rule > ply definitions > solid blade

As seen in figure 3.1.3, after applying the cut-off rule ply length varies from the longest at the bottom to the shortest ply at the top. As per the composite design rules elaborated above the ply drop rules are violated. Also as stated by Kemp et al. [7] interlamina and intralamina stresses increase at the location of ply drop. Plydrops closely spaced can thus cause stress concentration zones and need to be staggered between longer length plies. Xiao et al. [13] followed a shuffling approach to comply with the design rules. Shuffling of plies is thus also followed for the current project and is shown in figure 3.1.4

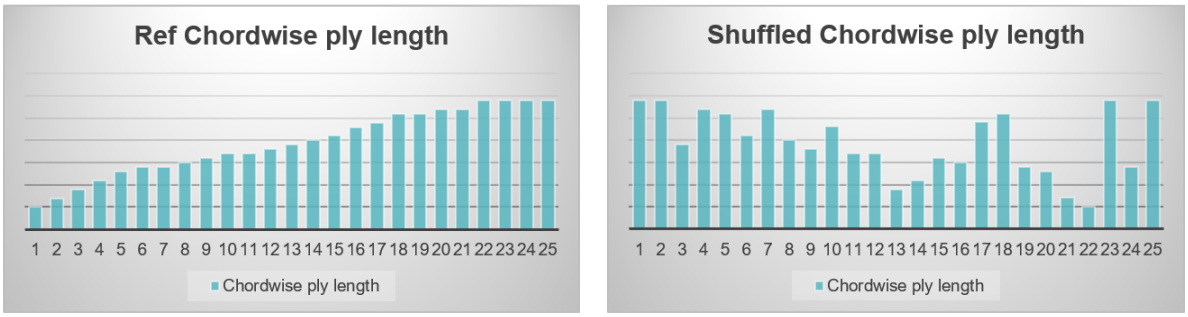

(a) Unshuffled plies (b) Shuffled plies

Figure 3.1.4: Unshuffled and Shuffled plies obtained using the offset parameter in the cut-off selection rule

Shuffling is achieved by changing the offset parameter in the cut-off selection rule. The offset parameter moves the pressure and suction surfaces in upward or downward direction in accordance to the value of offset. Thus the intersection of the plies with the bounding pressure and suction surfaces can be changed to vary the ply lengths. Thus it is possible to have a full length ply on the covering surface and shorter plies distributed within the stackup.

The methodology to define each ply in a modeling group has also provided the possibility to take advantage of the built-in excel interface in ACP module. Each ply defined in the modeling group both for suction and pressure side can be exported as an excel file. The excel file contains the information related to ply number, ply angle and the selection rules (cut-off selection rule in view of the current work) which can be altered in the excel format and pushed into the ACP module. This provides an easy way to alter ply stackup configurations and length of each ply by changing the parameter in the excel file. A picture of the excel file with the ply definitions is presented in figure 3.1.5

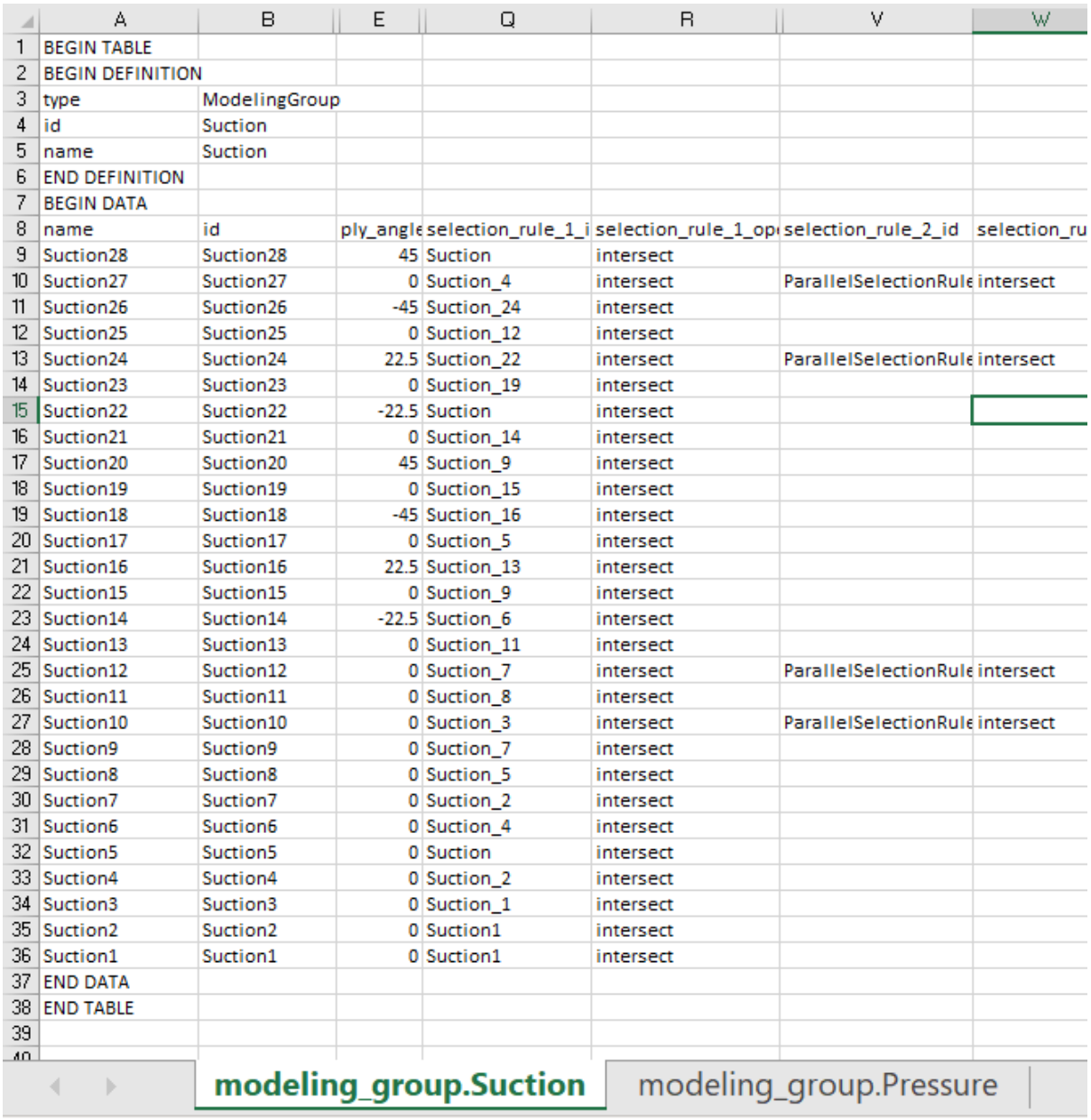

	A	B	E	Q	R	V	W
1	BEGIN TABLE						
2	BEGIN DEFINITION						
3	type	ModelingGroup					
4	id	Suction					
5	name	Suction					
6	END DEFINITION						
7	BEGIN DATA						
8	name	id	ply_angle	selection_rule_1_i	selection_rule_1_op	selection_rule_2_id	selection_ru
9	Suction28	Suction28	45	Suction	intersect		
10	Suction27	Suction27	0	Suction_4	intersect	ParallelSelectionRule	intersect
11	Suction26	Suction26	-45	Suction_24	intersect		
12	Suction25	Suction25	0	Suction_12	intersect		
13	Suction24	Suction24	22.5	Suction_22	intersect	ParallelSelectionRule	intersect
14	Suction23	Suction23	0	Suction_19	intersect		
15	Suction22	Suction22	-22.5	Suction	intersect		
16	Suction21	Suction21	0	Suction_14	intersect		
17	Suction20	Suction20	45	Suction_9	intersect		
18	Suction19	Suction19	0	Suction_15	intersect		
19	Suction18	Suction18	-45	Suction_16	intersect		
20	Suction17	Suction17	0	Suction_5	intersect		
21	Suction16	Suction16	22.5	Suction_13	intersect		
22	Suction15	Suction15	0	Suction_9	intersect		
23	Suction14	Suction14	-22.5	Suction_6	intersect		
24	Suction13	Suction13	0	Suction_11	intersect		
25	Suction12	Suction12	0	Suction_7	intersect	ParallelSelectionRule	intersect
26	Suction11	Suction11	0	Suction_8	intersect		
27	Suction10	Suction10	0	Suction_3	intersect	ParallelSelectionRule	intersect
28	Suction9	Suction9	0	Suction_7	intersect		
29	Suction8	Suction8	0	Suction_5	intersect		
30	Suction7	Suction7	0	Suction_2	intersect		
31	Suction6	Suction6	0	Suction_4	intersect		
32	Suction5	Suction5	0	Suction	intersect		
33	Suction4	Suction4	0	Suction_2	intersect		
34	Suction3	Suction3	0	Suction_1	intersect		
35	Suction2	Suction2	0	Suction1	intersect		
36	Suction1	Suction1	0	Suction1	intersect		
37	END DATA						
38	END TABLE						
39							

Figure 3.1.5: Excel interface with the ply definition like ply angle, selection rule

Chapter 4

Analysis and Cases

After building the model it is important to test the model for independence of the results on numerical parameters like mesh size. Here, the mesh definitions for the composite blade are provided on the camber surface which is then used to build the mesh for the solid model of the blade. To verify the mesh independence, results from modal analysis (Mechanical analysis) are analysed. Once a mesh independent blade model is achieved a number of ply stackup configurations are defined on which modal and blade flutter analysis is conducted. The blade flutter analysis gives the aerodynamic work which is used to calculate aerodynamic damping for each stackup and thus determines the stackup with flutter stability.

This section will first elaborate on the setup methodology used for the static, modal and blade flutter analysis. In the next section 5 results from the mesh independence study will be provided which will be followed by static structural, modal and aerodamping results for each stackup.

4.1 Setup for Mechanical analysis

The Mechanical analysis setup includes the static structural analysis and the pre-stressed modal analysis. The static structural module (D) follows the ACP-Pre module (C) which is then followed by the modal module (E). The setup flow for Mechanical analysis can be seen in figure 4.1.1 in blocks C, D and E.

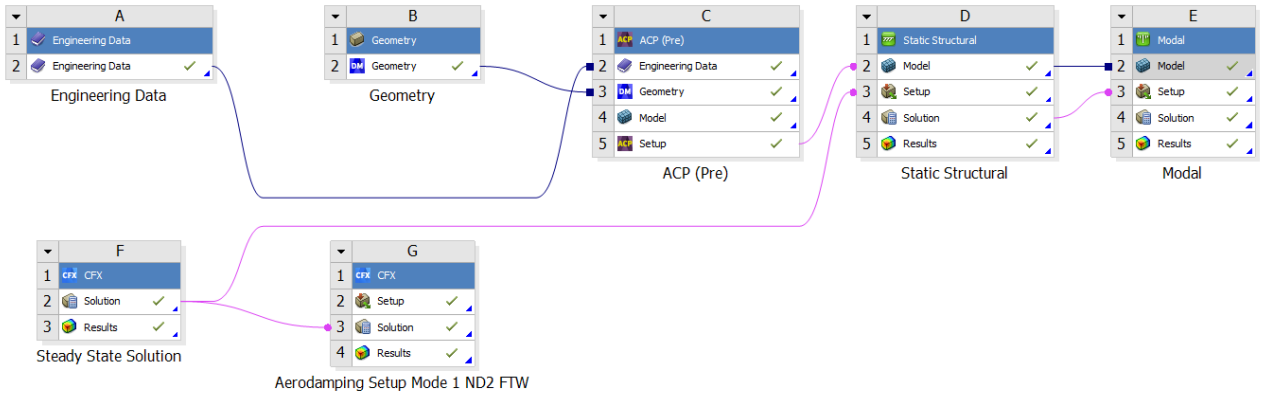

Figure 4.1.1: Setup methodology used for the investigations in the thesis.

4.1.1 Static structural module

The methodology to build the composite blade in ACP is detailed in section 3.1. The static structural module is then inserted in workbench. The composite model which is built in the ACP-Pre module is dragged from the ACP-Pre setup cell to the Static structural Model cell and the transfer type option is chosen as solid model.This operation imports the composite blade model with all the individual ply definitions as set in the modelling groups in ACP-Pre into static structural under the imported plies group. The geometry information, material details, mesh , coordinate system are all imported from the ACP module. The named selections are automatically generated based on the solid geometry. Two additional named selections are created at this stage for the blade pressure side and blade suction side by duplicating the blade top and bottom surfaces from the default named selections. This named selections will be used during the modal analysis for extraction of the mode shapes.

At this stage we define the structural analysis settings, boundary conditions and the required result output. The analysis settings determine the type of solver, time stepping settings, solver controls, output controls as some of the controls. The Large deflection setting is turned on as recommended in Ansys documentation [3]. The files are retained after full solve using the Restart controls. Future analysis is set to ”Prestressed analysis” for the following modal analysis. The other settings in the analysis settings tab are set to default and will be program controlled. The boundary conditions are now set for the blade. The fixed support is defined at the hub surface of the blade. This operation leads to the assumption that the blade is perfectly attached to the disk and the disk is a perfectly rigid, meaning the simulation considers a blade

dominated zone. Also there are no non-linear effects due to friction between the dove tail and the disk. As the current study is focused on flutter stability which is largely influenced by damping the fixed support assumption is conservative as any friction would act as damping contribution leading to stability of the system. Next the rotational velocity is specified with reference to the global coordinate system. The Z-axis represents the machine axis with the flow moving in the positive Z-direction. The X-axis specifies the radial direction and the Y-axis perpendicular to both axis. A positive rotational velocity of 7454 rpm is specified about the Z-axis which according to right-hand convention imposes a clockwise rotation when seen from the inlet to the positive Z-axis. The rotational velocity introduces the centrifugal stiffening effect which is later used in the prestressed modal analysis. As seen in figure 4.1.1 a steady state CFX solution (F) is connected to setup cell of static structural module (D). This imports the steady-state pressure and thus can be specified on the blade under the ”Imported load” tab. A pressure load is inserted under the imported load, the blade pressure and suction surfaces are defined as geometries where the load is to be imposed. Total static deformation is inserted as the required solution. The static structural analysis is now solved. A pictorial representation of the setup for static structural and modal analysis is placed in figure 4.1.2

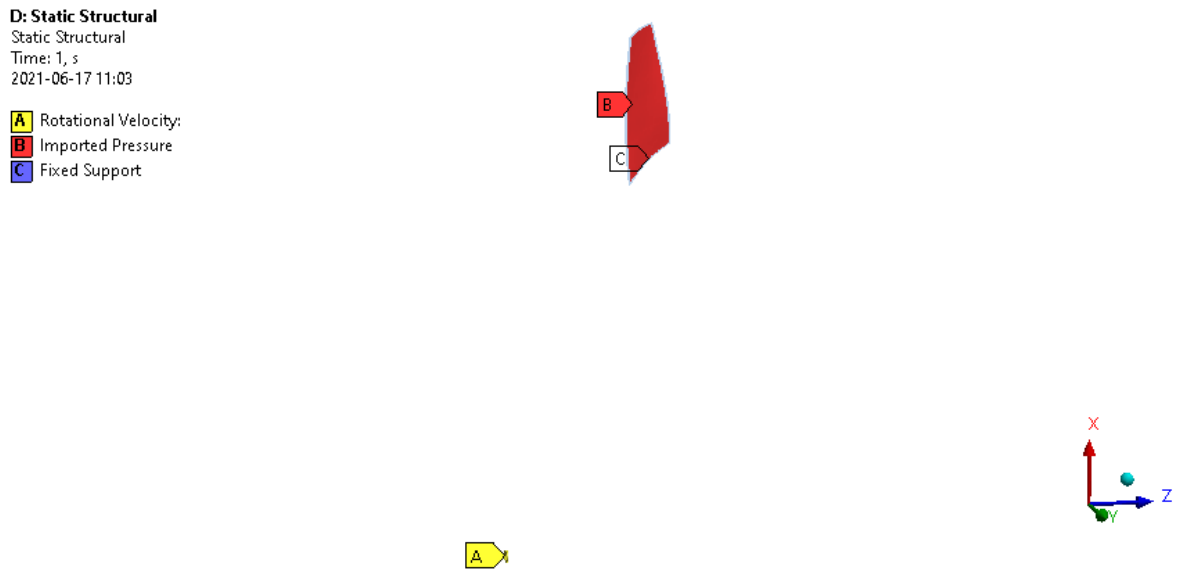

Figure 4.1.2: Setup for Mechanical analysis with the prescribed boundary conditions

4.1.2 Pre-stressed modal module

After the solution for static structural (D) analysis is obtained the solution is transferred to the modal module (E). The modal analysis accounts for the stiffening due to centrifugal and pressure loads. In the analysis settings the maximum number of modes desired in the study are specified. The damping is set to none thus assuming zero structural damping. This is inline with the findings of Srinivasan [4] where material damping was found to be very small as compared to aerodynamic damping. Other settings are left to default options. The mode shapes that will be obtained after solving the modal analysis need to be exported so as to impose them later in the aerodamping setup (G). To export the mode shapes an Ansys APDL script is provided as command in the modal solution. The commands are listed in the Appendix A.

4.2 Setup for Blade flutter analysis

The aeroelastic stability of a stackup for a particular vibration mode can be determined from the aerodamping values under the operating conditions. The aerodamping values can be obtained by performing a blade flutter analysis in Ansys CFX. The methodology is illustrated in Ansys documentation [3] and will be described here.

The important factors influencing the aerodamping values are the vibration mode and the nodal diameter of the disk. The theory on nodal diameters and the corresponding Inter-blade phase angle (IBPA) are described in section 2.3. The IBPA determines the phase difference between the adjacent blades and thus influences the aerodynamic coupling. In the investigated case there are 37 blades on the disk which account for a maximum of 18 nodal diameters each in backward and forward travelling as per the equation 2.17 in section 2.3. The blade flutter analysis is required to be conducted for each nodal diameter to determine the nodal diameter of least stability.

The transient blade row blade flutter simulation using time integration in combination with Fourier transformation pitch change model is used as illustrated in tutorials provided in Ansys documentation [3]. In case of standard rotational periodicity conditions, the number of passages required to be modelled to perform a transient blade row simulation are dependent on the nodal diameter under investigation. Also the domain can be reduced only when the the number of blades on the disk are an integer multiple of the nodal diameter. In absence of which the whole blisk is

required to be modelled. In case the the number of blades is integer multiple of nodal diameter the number of passages can be reduced to integer multiple value to ensure rotational periodicity. However with the option of Fourier transformation the number of domains can be reduced to a minimum of 2 for any nodal diameter. In the Fourier transformation method CFX collects the information of the flow field on the common interface of the two blade passages and phase shifts the information and applies on the periodic boundaries. This leads to phase-shifted periodic boundaries leading, lagging or in-phase with the common interface. The transient simulation also requires a initial solution to guarantee convergence of results. Hence first a steady state simulation is run and the results are used to initialise the transient flutter analysis.

4.2.1 Steady state setup

The CFX mesh definitions with a resolved mesh are available for the current project. Thus mesh independence study of CFX mesh is not a part of this study. The CFX module is inserted in the workbench flow and the CFX-Pre setup is started. In the tools option the turbo mode is started to define the mesh, domains and boundary conditions. In the basic settings the machine type is set to axial compressor with the rotation axis as Z in the global coordinate system. The type of analysis chosen is the steady state. Now the components of the model which is the rotor is inserted in the component definition and the type is specified as rotating and rotation speed is specified. The rotor mesh file is specified under the mesh file tab. For Fourier transformation, two domains are required hence the passages to model is selected as 2 and passages in 360 are selected as 37. Next in the physics definitions the fluid is chosen as air ideal gas, the heat transfer as total energy and the turbulence model as k-epsilon. The turbulence model k-epsilon selected for the project is in view of lower CPU time and the primary objective being the variation in mechanical behaviour due to changes in the composite stackup. The inlet boundary conditions are set to total pressure and the outlet to static pressure. The values are left to default and are later imposed with profile data option. The inlet and outlet boundary profiles are available and extracted from the simulations done for the complete compressor model. The simulation of complete compressor is not in scope of this thesis and only the final results are used to extract the boundary conditions profiles. The periodic interfaces are now defined and the common interface between two passages is defined as none type interface. Finally the number of passages modelled is set to 2 and number of total passages is set to 37 and the Turbo setup is

finished. The profile data for inlet and outlet boundary condition is imported using the initialise profile data option from the tools menu. Similarly the mode shape is also imported and then using the edit profile data option it is transformed to the complete 360 circle using expand profile data method. The blades in both passages are grouped together in one blade domain for the Fourier transformation method. The frame type for the inlet and outlet surfaces is specified as stationary and for the blade, hub, shroud and interfaces as rotating. The profile data option is turned on for the inlet, outlet and blade domains and the values are generated. For the steady state case the mesh motion of the blade is specified as stationary. The mesh motion of inlet, outlet, hub and the interfaces is also specified as stationary. For the shroud the mesh motion is specified as surface of revolution and the wall velocity is defined as a counter rotating wall. The setup is saved and the solution is solved with a double precision option. The above description gives an overview of the CFX setup methodology and for more details the Ansys documentation [3] can be referred. It is to be noted that in the above procedure the tip gap between the blade tip and the shroud is not specified and thus the analysis is performed with the assumption of no tip gap. This is a part of future work where the effect of tip gap can be investigated.

4.2.2 Transient blade flutter setup

For the transient blade row setup the steady state setup is duplicated and used as a starting point. The analysis type is changed to transient blade row. The mesh deformation option for the rotor domain is set to regions of motion specified and relative to the initial mesh. The mesh motion for the blade boundary is specified as periodic displacement in Cartesian components. By generating the values in the basic settings tab mesh motion is automatically imposed. The scaling factor is set to allow a maximum mesh displacement of 0.001 m. This value ensures that the mesh motion does not lead to negative volumes. The phase angles between the blades is specified by the nodal diameter and the travelling wave direction. The transient blade row settings are provided at this stage. The type for transient blade row is set to Fourier transformation. Blade flutter is selected as the required analysis and the sampling and periodic interfaces are specified. The blade boundary is set as the blade domain and the time period, time steps and period per run are set to the recommended values as per CFX. Next the output controls are set to specify aerodynamic damping as an output parameter in the solver output. This gives the aerodynamic damping work over one

vibration cycle in the output monitor. The final value at the end of the solution is the value of interest. The convergence of the solution can be verified by the values of aerodamping work on each blade which should be within an acceptable tolerance. To monitor convergence of results the torque on the each blade is also monitored in the solution monitor. As per CFX recommendation a converged solution for a fourier transform blade flutter analysis is obtained within 3-6 cycles of vibration.

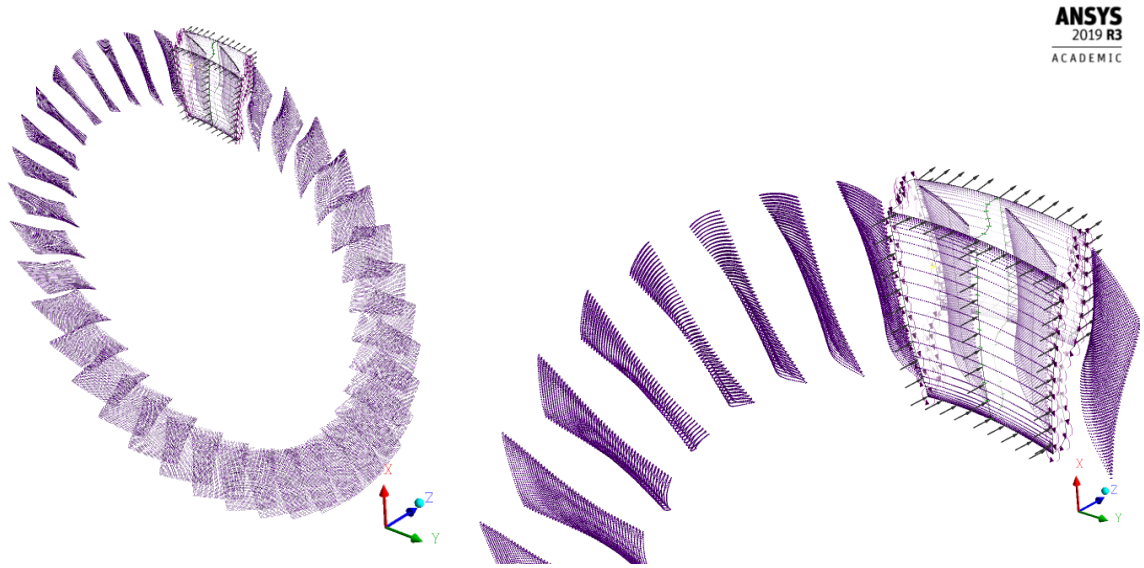

(a) (b)

Figure 4.2.1: CFX setup for blade flutter analysis representing 2 domains used for analysis and the mode shape imposed on the blade surface

4.3 Investigated cases

This section presents the cases investigated in the scope of this thesis. The stackup configurations are decided based on the literature study presented in section 1.1. A range of ply angles between 0° to 45° with a step of 15° were investigated by Reiber et al. [9]. Xiao et al. [13] used a combination of 0° and 45° plies. Wollman et al. [19] stated that the 0° plies take up the longitudinal loads while 45° plies take up the torsional loads. In view of this in current projects stackups are generated by using 0°, 22.5°, 45° and 60° plies. The 60° plies are investigated to look on effect of going beyond the ply angle of 45°. The investigated stackup configurations on one side of the symmetry line are presented in table 4.3.1. The ply number 1 is the outer most ply placed on either the suction or pressure surface while the ply 25 is placed on the camber surface.

	Stackup					
Ply no	**1**	**2**	**3**	**4**	**5**	**6**
1	60	45	22.5	45	45	45
2	45	22.5	0	0	45	45
3	22.5	0	-22.5	-45	0	22.5
4	0	-22.5	-45	0	-45	0
5	-22.5	-45	-22.5	45	-45	-22.5
6	-45	0	0	0	0	-45
7	-60	45	22.5	-45	45	-45
8	-45	22.5	45	0	45	-22.5
9	-22.5	0	0	45	0	0
10	0	-22.5	-45	0	-45	0
11	22.5	-45	0	-45	-45	45
12	45	-22.5	45	0	0	22.5
13	0	0	0	45	0	0
14	0	0	0	0	0	0
15	-60	22.5	22.5	-45	45	22.5
16	-22.5	45	45	0	45	-22.5
17	0	0	0	45	0	-45
18	0	0	0	0	0	0
19	0	-45	-45	-45	-45	-22.5
20	0	-22.5	-22.5	0	-45	0
21	22.5	22.5	22.5	-45	0	22.5
22	-22.5	-22.5	-22.5	0	0	-22.5
23	0	45	0	45	45	0
24	22.5	22.5	22.5	0	0	22.5
25	60	0	0	0	45	0

Table 4.3.1: Investigated stackups to study the effect of changing ply orientation on the flutter stability

Chapter 5

Results

In this section the mesh independence study will be presented first to conclude on the reliable model of the blade. Then the static structural results will be presented followed by the aerodamping results corresponding to each stackup first for Mode 1 and later for Mode 2. The observed relation between the stackup sequence and the aerodamping will be elaborated.

5.1 Mesh Independence study

A reference stackup with all 0° plies is used for mesh independence study. The mesh element size on the camber surface is varied from 4 mm to 2 mm with all other parameters as mentioned in section 3.1 kept unchanged. The starting size of 4 mm was chosen as it was the minimum size which provided a mapped quadrilateral mesh. The modal analysis results for each mesh size are used for concluding the mesh independence. The modal frequencies for the first 2 modes against the number of nodes is plotted in the figure 5.1.1a and 5.1.1b and the CPU time required for the simulation is presented in figure 5.1.1c. The values are tabulated in table 5.1.1

Mesh Size [mm]	No. of nodes	Mode 1 [Hz]	Mode 2 [Hz]	Mode 3 [Hz]	CPU time [min]
4	105125	476.24	633.4	962.36	6.16
3	186918	478.37	638.03	962.39	8.44
2	404415	482.47	642.95	971.29	89.46

Table 5.1.1: Modal frequency and CPU time results from Mesh independence study

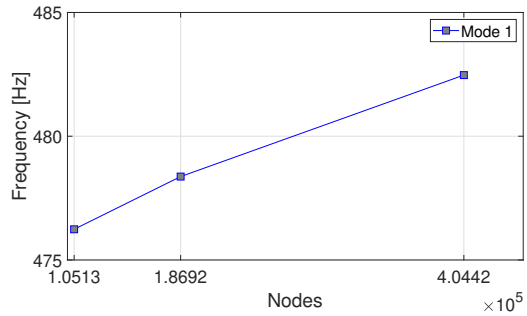

(a) Frequency for the Mode 1 of vibration for mesh size of 4mm, 3mm and 2 mm

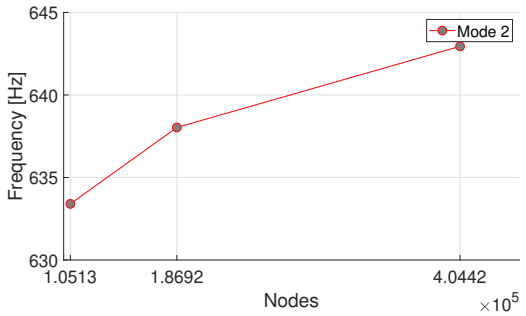

(b) Frequency for the Mode 2 of vibration for mesh size of 4mm, 3mm and 2 mm

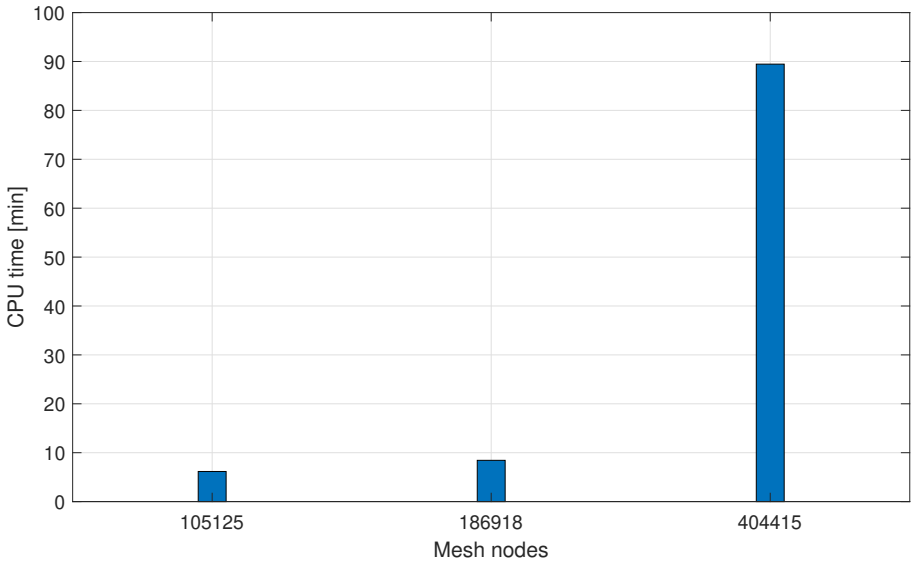

(c) CPU time for the mesh size of 4mm, 3mm and 2 mm

Figure 5.1.1: Frequency and CPU time results for mesh independence study

From the results it is evident that the all 3 mesh provide a converged results with a maximum variation of 1.5 % in the frequency values. The CPU time however is significantly higher for the mesh size of 2 mm. The probable reason along with a higher mesh size is the hardware limitations on the system being used for simulations. As the time taken and results from the 3 mm and 4 mm surface mesh are well within reasonable limits the 3 mm mesh is opted for the simulations in the project.

Further referring to documentation in Ansys [3] it is suggested to use multiple elements per ply thickness to ensure accurate simulation. A check is thus performed to investigate the influence of multiple elements/ply on the results and the results are presented in table 5.1.2 and figure 5.1.2

Elements/ply	No. of nodes	Mode 1 [Hz]	Mode 2 [Hz]	Mode 3 [Hz]	CPU time [min]
1	186918	478.37	638.03	962.39	8.44
2	369054	478.39	638.08	962.35	100.16

Table 5.1.2: Modal frequency and CPU time results for multiple elements per ply

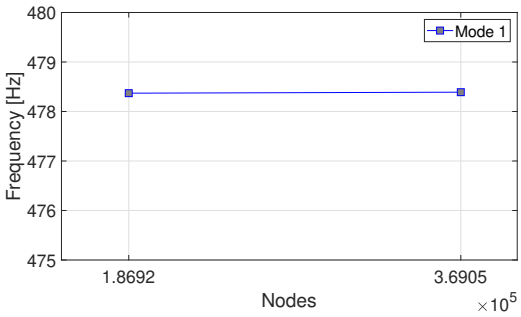

(a) Frequency for the Mode 1 of vibration for 1 element/ply and 2elements/ply

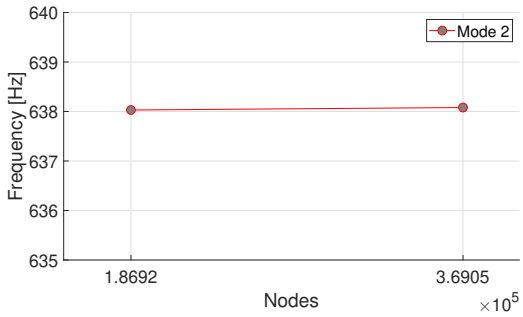

(b) Frequency for the Mode 2 of vibration for 1 element/ply and 2elements/ply

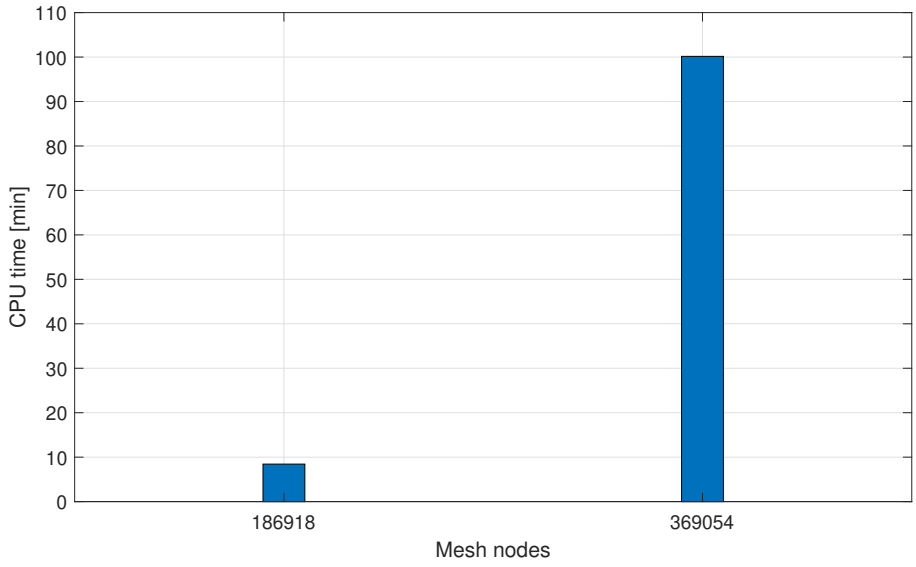

(c) CPU time for the 1 element/ply and 2elements/ply

Figure 5.1.2: Frequency and CPU time results for elements/ply independence study

The increase in number of elements/ply is observed to have negligible effect on the results. The study on the surface mesh size and the number of elements per ply thus provides a reliable model providing converged results.

Next taking a look at the distribution of ply drops in the stackup it is observed that few plies have a considerably shorter length. It is of interest to check the contribution of these plies to the overall vibration behaviour. This is done by assigning a 45° angle to ply number 13, 14, 19, 20, 21 and 22 while other angles are maintained at 0° angle

same as the reference configuration. This stackup is referred as Stackupshort. A comparison of this stackup is made with reference stackup. The selected shorter plies are highlighted in figure 5.1.3 and the results are compared to reference stackup in table 5.1.3

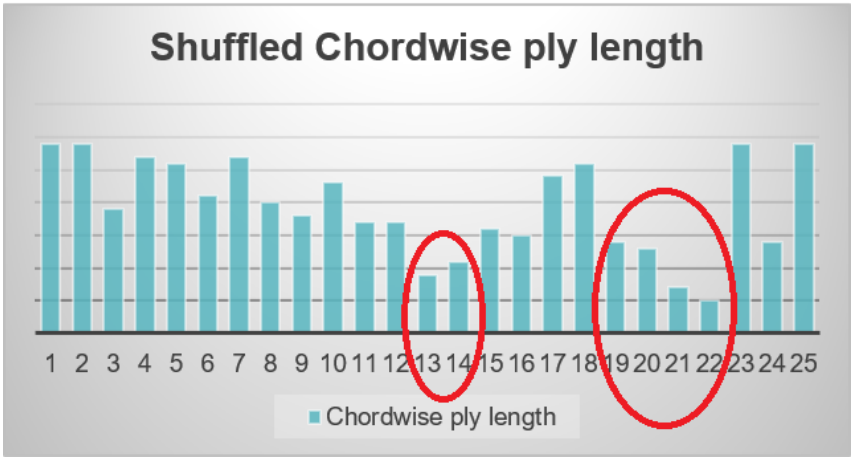

Figure 5.1.3: Investigating the contribution of shorter plies on the overall frequency of the blade

	Mode 1 [Hz]	**Mode 2 [Hz]**	**Mode 3 [Hz]**
Stackupshort	478.37	638.03	962.39
Reference stackup	480.01	626.33	962.42

Table 5.1.3: Contribution of shorter plies on the overall frequency of the blade

It can be seen that the highlighted short plies have a maximum of 1.8 % variation in the Mode 2 frequency and very negligible effect on the other two modes.Thus they majorly serve the purpose of adjusting the overall composite structure to the blade shape. Thus while changing the ply angles and deciding the stackup the focus is kept on the stacking sequence of the longer plies on the outer surface of the stackup.

5.2 Static structural analysis results

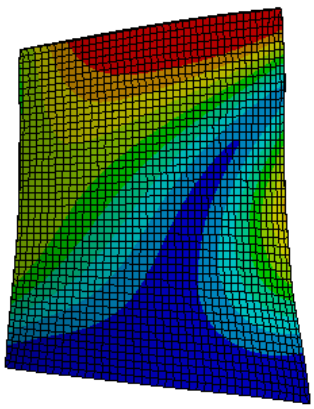

(a) Stackup 1, Max disp:0.69 mm

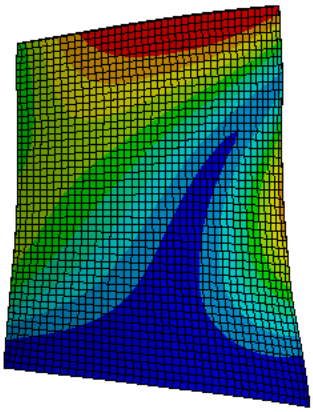

(b) Stackup 2, Max disp:0.64 mm

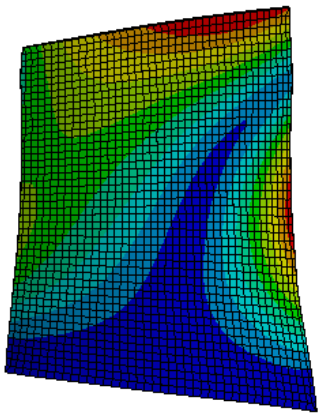

(c) Stackup 3, Max disp:0.59 mm

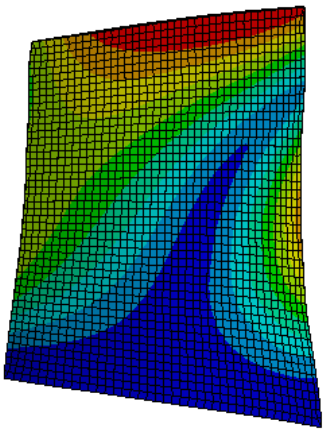

(d) Stackup 4, Max disp:0.62 mm

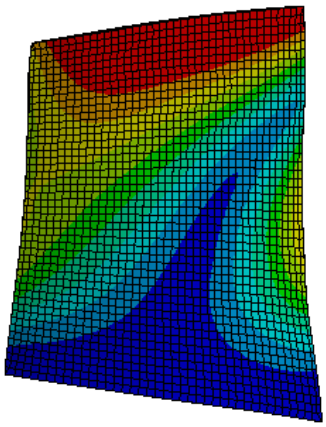

(e) Stackup 5, Max disp:0.74 mm

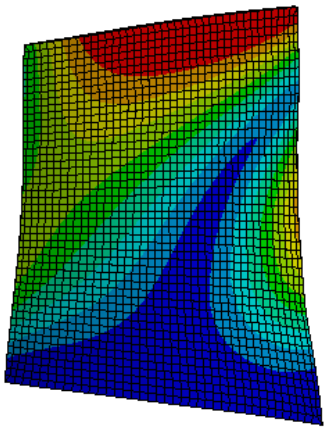

(f) Stackup 6, Max disp:0.70 mm

Figure 5.2.1: Static structural results for Stackup 1 to Stackup 6

The results from the static structural analysis are presented in figure 5.2.1. The color representation is adjusted to show in red any displacement above a value of 0.5 mm. The maximum deflection is observed to occur near the leading edge tip region. The maximum static displacement is observed for Stackup 5 which has a higher number of $\pm 45^\circ$ plies in the stackup and 45° ply on the outer surface. The minimum is observed for Stackup 3 which has higher number of $\pm 22.5^\circ$ plies in stackup and 22.5° ply on the outer surface. Stackup 4 having a higher number of 0° plies in the stackup and 45° ply on the outer surface shows the second lowest static displacement. Thus lower value of ply angles in the stackup and their placement on outer surface is seen to result in lower static displacement value. The maximum value of static displacement observed across all stackups is 0.74 mm.

5.3 Modal analysis results

The results of the modal analysis provide the mode shapes and the modal frequencies for each stackup. The 1st two modes are of interest and presented in figure 5.3.1

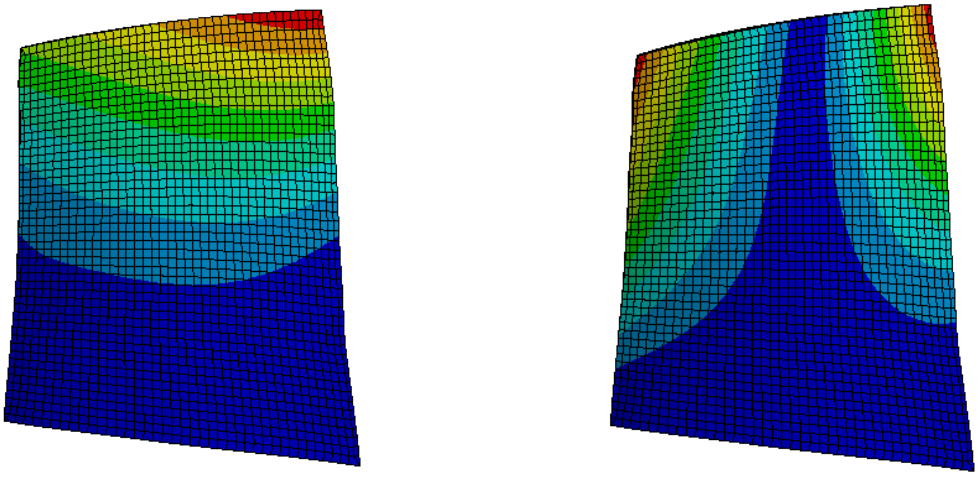

(a) Mode 1 (b) Mode 2

Figure 5.3.1: 1st two modes obtained from the modal analysis

It is observed that the 1st mode exhibits a bending like behaviour and 2nd mode a torsion like behaviour. It is of interest to look at the mode shape and frequency for each stackup and their relation with the stackup. To understand the effect of the ply angle configuration on the mode shape and frequencies a relation between the stackup shear and longitudinal stiffness with the twisting at the blade tip and modal frequency is investigated. The twisting is calculated from the blade tip edge to edge deflection of mode. The stiffness here is calculated according to classical laminate theory for an equivalent laminate with no ply drops as represented in figure 2.1.3 and having the ply stackup configuration as of the investigated stackups. The stiffness values do not represent the actual stiffness values of the blade but represent a stiffness value of one equivalent mesh element encompassing the investigated stackup configuration. The stiffness term A_{11} is the longitudinal term while the term A_{66} is the pure shear term of inplane stiffness while D_{11} and D_{66} are the out of plane terms. It is to be noted that the red color highlighting the maximum displacement is adjusted in Mode 1 to highlight displacement above 11.82 [-] and for Mode 2 above 15.423 [-]. The displacements are mass orthonormalised displacement values obtained from the modal analysis. Any part of blade with deflection above this values will be shown in red.

5.3.1 Mode 1

The 1st mode shows a maximum deflection at the leading edge tip thus there is portion of twisting present in the mode shape along with the classical bending mode. The mode shapes for the Stackup 1 to Stackup 6 are presented in figure 5.3.2. This gives a visual understanding of the deflection of the blade for each stackup.

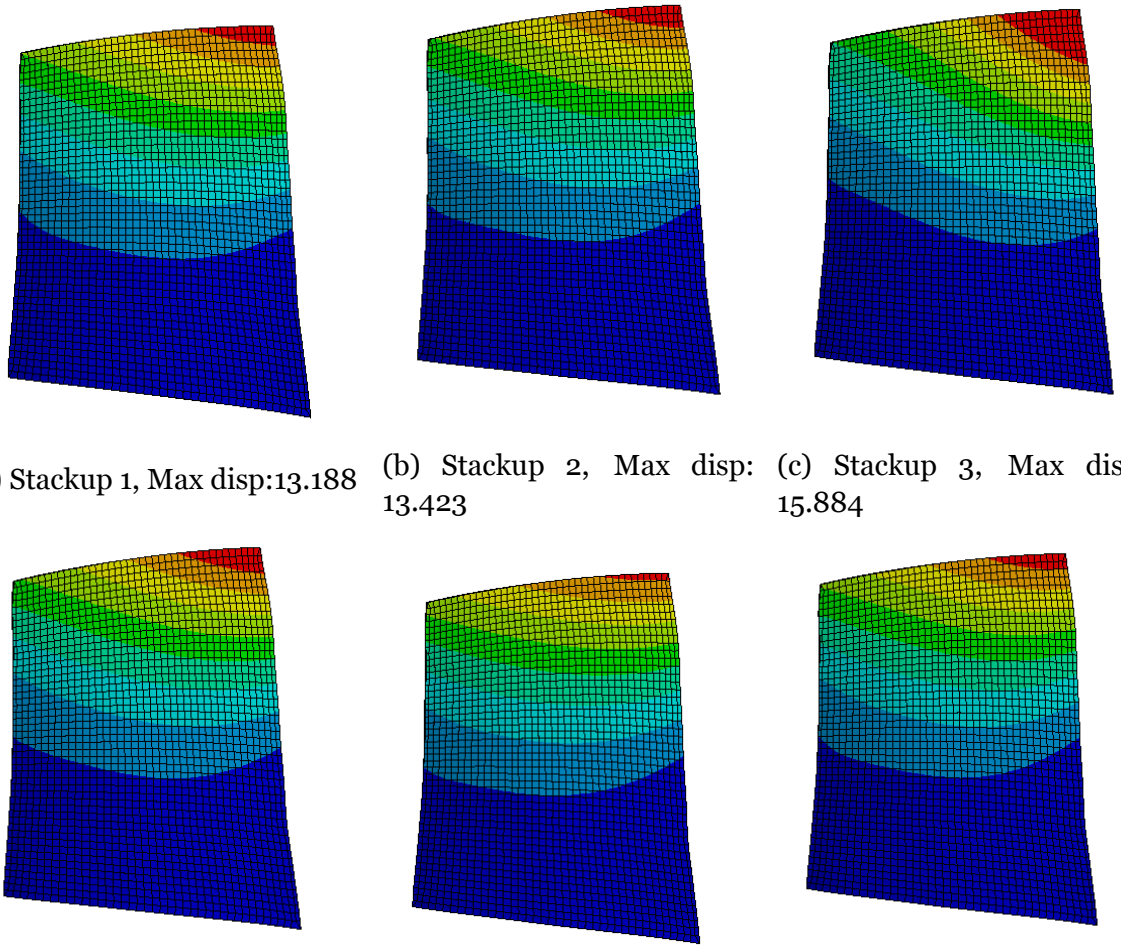

(a) Stackup 1, Max disp:13.188

(b) Stackup 2, Max disp: 13.423

(c) Stackup 3, Max disp: 15.884

(d) Stackup 4, Max disp: 13.69

(e) Stackup 5, Max disp: 12.3

(f) Stackup 6, Max disp: 12.956

Figure 5.3.2: 1st mode for Stackup 1 to Stackup 6

It is observed that Stackup 3 has the highest deflection and Stackup 5 the lowest. The deflection of other stackups is in between these two stackups. Also observing the mode shape the deflection in Stackup 3 is concentrated at the leading edge tip of the blade. In Stackup 5 the deflection is seen to be maximum at the leading edge tip but with a gradual distribution away from the leading edge tip compared to Stackup 3. To further look at the relation between stiffness values and mode shape the stiffness terms A11,

A66, D11 and D66 are plotted against the twisting at the tip for each stackup in figure 5.3.3. Comparison of stiffness terms and frequency is given in figure 5.3.4.

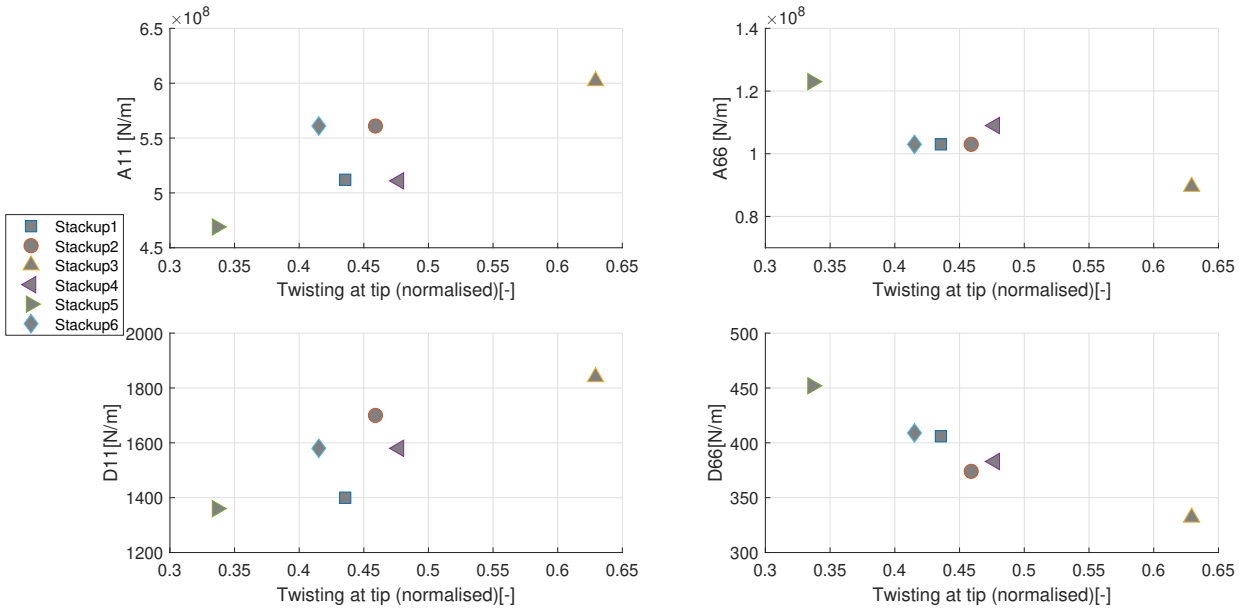

Figure 5.3.3: Stiffness terms A11, A66, D11 and D66 plotted against the twisting at tip for Mode 1

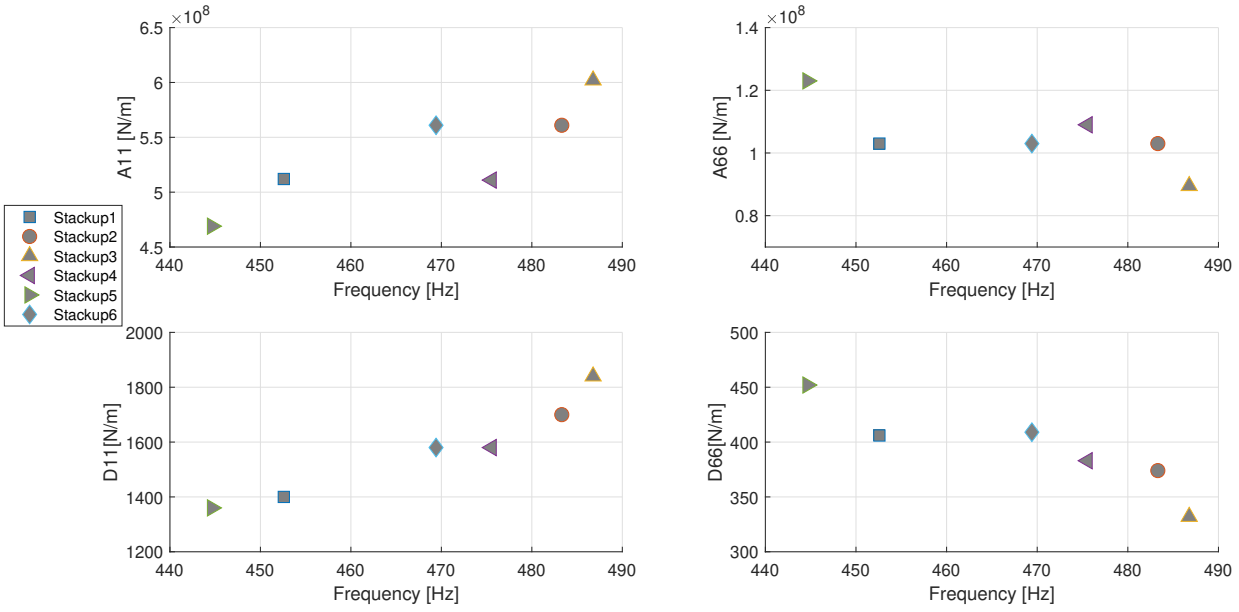

Figure 5.3.4: Stiffness terms A11, A66, D11 and D66 plotted against the modal frequency for Mode 1

Stackup 5 with the highest shear stiffness A66 and lowest longitudinal stiffness A11 has the lowest twisting at the tip present in its mode shape. The lowest longitudinal

stiffness also results in the minimum value of Mode 1 frequency which is the bending mode. Stackup 3 with the lowest shear stiffness A66 and highest longitudinal stiffness A11 has the highest twisting present in its mode shape. The highest longitudinal stiffness leads to the highest bending mode frequency for Stackup 3. The other stackups have twisting values between 0.4 [-] to 0.5 [-]. These stackups do not represent a strong trend between stiffness and twisting as observed in Stackup 3 and Stackup 5. This can be due the stiffness matrix of the actaul blade being different than the stiffness of an ideal laminate due to the ply drops and varying length of plies.

To further establish the link between the stackup configuration, its stiffness and finally its mode tip twisting and frequency we look at the ply angles, the number of plies of a particular angle and the placement with respect to symmetry axis. The ply angles making up each stackup and the number of plies of each angle are presented in table 5.3.1a. From theory it is known that the out of plane stiffness terms are affected by the position of ply. Thus the angles on the outermost plies have a more significant effect on the stiffness behaviour. Thus the number of plies for each angle present in the outermost 12 plies is presented in table 5.3.1b.

	Stackup					
Ply Angle	**1**	**2**	**3**	**4**	**5**	**6**
0	9	9	11	13	11	9
22.5	4	5	5	0	0	5
-22.5	4	5	5	0	0	5
45	2	3	2	6	7	3
-45	2	3	2	6	7	3
60	2	0	0	0	0	0
-60	2	0	0	0	0	0

(a)

	Stackup					
Ply Angle	**1**	**2**	**3**	**4**	**5**	**6**
0	2	3	4	6	4	3
22.5	2	2	2	0	0	2
-22.5	2	3	2	0	0	2
45	2	2	2	3	4	3
-45	2	2	2	3	4	2
60	1	0	0	0	0	0
-60	1	0	0	0	0	0

(b)

Table 5.3.1: a) Number of plies of each angle in the investigated complete stackups b)Number of plies of each angle in the outer 12 plies of the investigated stackups

Stackup 5 configuration which looks like $[(45/45/0/-45/-45/0)_2/...]_s$ on the outermost 12 plies has higher number $\pm 45^\circ$ plies thus a higher shear stiffness leading to lower twisting and lower longitudinal stiffness leading to lower bending frequency. Stackup 3 which looks like $[22.5/0/-22.5/-45/-22.5/0/22.5/45/0/-45/0/45/...]_s$ has lower number of $\pm 45^\circ$ and higher number of $\pm 22.5^\circ$ plies thus having lower shear stiffness leading to higher twisting and higher longitudinal stiffness leading to higher frequency. Comparing the overall stackup of Stackup 3 with Stackup 2, Stackup 3 has higher 0°

and lower $\pm 45^\circ$ plies than Stackup 2. On the outermost 12 plies of both stackups both have same number of $\pm 45^\circ$ plies but the number of 0° plies is higher in Stackup 3. Furthermore, Stackup 2 which is $[(45/22.5/0/\text{-}22.5/\text{-}45)/0/(45/22.5/0/\text{-}22.5/\text{-}45)/\text{-}22.5/...]_s$ has 45° plies towards the outer surface while Stackup 3 has 22.5° plies towards the outer surface. Thus higher number of plies with lower ply angle and placement of those plies towards the outer surface leads to lower shear stiffness leading to higher twisting and higher longitudinal stiffness leading to higher frequency for Stackup 3. Comparing Stackup 3 with Stackup 4 which is $[(45/0/\text{-}45/0)_3/...]_s$, Stackup 4 has higher number of both $\pm 45^\circ$ and 0° plies than Stackup 3. In the overall Stackup 4 the number of $\pm 45^\circ$ is considerably higher. The 5 pairs of $\pm 22.5^\circ$ plies in Stackup 3 are replaced by 4 pairs of $\pm 45^\circ$ plies in Stackup 4. The presence of higher number of $\pm 45^\circ$ plies thus leads to higher shear stiffness and lower twisting, and lower longitudinal stiffness and lower frequency for Stackup 4. Comparing Stackup 2 with Stackup 6, both have the same number of each ply angle in the overall stackup and thus same value for A11 and A66 terms. However on the outermost 12 plies the number of $+45^\circ$ ply angle is higher for Stackup 6 which gives it a higher value of stiffness D66 and thus a lower twisting. It also leads to a lower value of stiffness D11 and thus a lower frequency. Stackup 1 which has a pair of $\pm 60^\circ$ plies is also seen to have lower frequency and lower twisting. The stackup which offers a good balance between lowering the twisting and increasing the frequency is Stackup 6 and Stackup 2 which have a good balance of $\pm 45^\circ$, $\pm 22.5^\circ$ and 0° plies in the overall stackup and also towards the outer surface of stackup. Thus it can be inferred that to have a lower twisting it is important to have higher number of 45° plies and lower number of 0° and $\pm 22.5^\circ$ plies on the outer side of the stackup and the opposite to have a higher frequency. To achieve an optimum stackup these plies are required to be evenly distributed as in Stackup6 and Stackup 2.

5.3.2 Mode 2

As done for the Mode 1 the mode shapes of Mode 2 for the Stackup 1 to Stackup 6 are presented in figure 5.3.5.

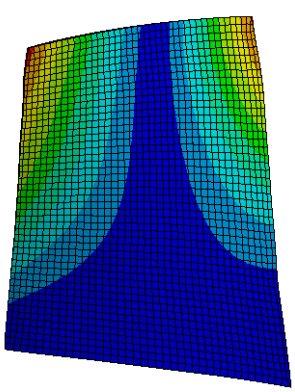

(a) Stackup 1, Max disp:16.407

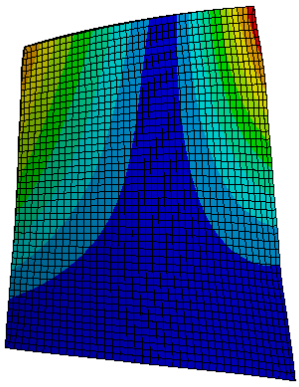

(b) Stackup 2, Max disp: 17.028

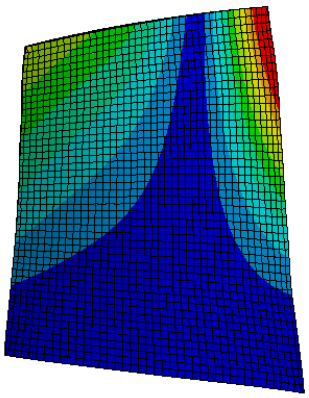

(c) Stackup 3, Max disp: 20.733

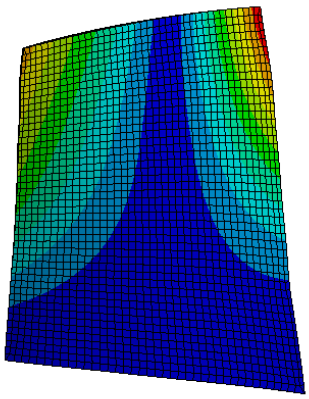

(d) Stackup 4, Max disp: 17.351

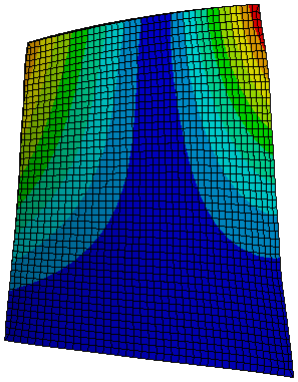

(e) Stackup 5, Max disp: 17.368

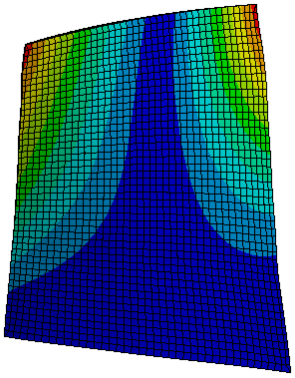

(f) Stackup 6, Max disp: 16.641

Figure 5.3.5: 2nd mode for Stackup 1 to Stackup 6

All stackups show a inflection line along the span of the blade indicating a torsional mode. The position of inflection is seen to move towards the leading edge (right) in Stackup 3 and the deflection can be seen distributed over a larger portion of the leading edge. The trailing edge of Stackup 3 however does not show much deflection. Stackup 1 is seen to have a higher deflection on the trailing edge as compared to the leading edge.

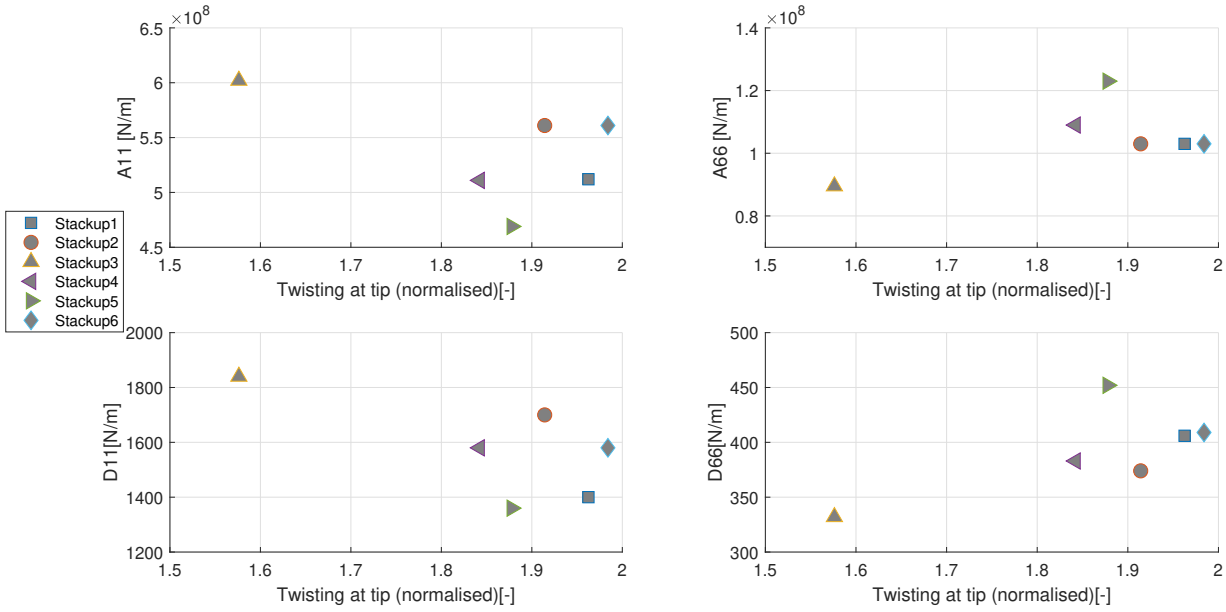

Figure 5.3.6: Stiffness terms A11, A66, D11 and D66 plotted against the twisting at tip for Mode 2

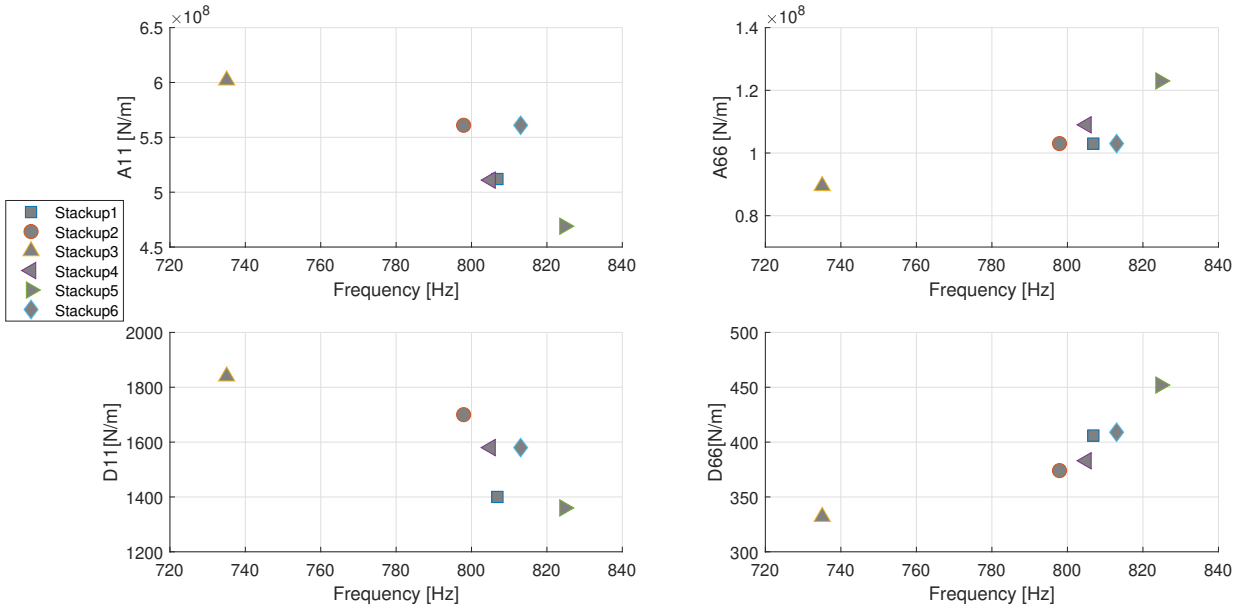

Figure 5.3.7: Stiffness terms A11, A66, D11 and D66 plotted against the modal frequency for Mode 2

From figure 5.3.6 it can be seen that the Stackup 3 with the lowest shear stiffness and highest longitudinal stiffness shows the lowest twisting. Also Stackup 5 with the highest shear stiffness and lowest longitudinal stiffness does not show the lowest twisting. This is in contrast to the observation in Mode 1. A strong correlation between

the stiffness values and the twisting present at the tip cannot be established from the above figures. Looking at the stackup configuration and table 5.3.1a and table 5.3.1b, Stackup 3 with lowest twisting has higher number of $\pm 22.5^\circ$ and 0° plies. The second lowest twisting is observed for Stackup 4 which has a relatively higher number of 0° plies. Thus it can only be commented that ply angles of lower value and their placement on the outer surface is observed to have lower twisting in the mode shape. This is further elaborated in the discussion of aerodamping results with figures of the mode shape in section 5.4.2.

Observing the stiffness vs frequency plot in 5.3.7, Stackup 3 with the lowest shear stiffness has the lowest frequency while Stackup 5 with the highest shear stiffness has the highest frequency. Here, $\pm 45^\circ$ and their placement towards the outer surface of the stackup tends to maximize the shear stiffness A66 and D66 and thus have a higher frequency.

5.4 Aerodynamic damping

After analysing the modes and the effect of stackup configuration on the mode behaviour, the effect of stackup on aerodynamic damping for Mode 1 and Mode 2 will be investigated in this section. The aerodynamic damping work values are obtained from the blade flutter analysis explained in section 2.2. The aerodynamic damping is a scaling of the aerodynamic work per blade vibration cycle. A number of scaling methodologies are proposed in various literature. In the current project the aerodynamic work is scaled using the kinetic energy of blade vibration [1]. The damping factor and the damping ratio are calculated using equation 5.1 and 5.2 respectively.

$$\delta = \frac{W_{aero}}{4.K.E} = \frac{W_{aero}}{4.\frac{(s\omega)^2}{4}} \tag{5.1}$$

$$\xi = \frac{\delta}{2\pi} = \frac{W_{aero}}{2\pi(s\omega)^2} \tag{5.2}$$

where damping factor (δ) is the aerodynamic work per cycle (W_{aero}) divided by the kinetic energy of blade vibration (K.E). The kinetic energy is related to the scaling (s) and the blade vibration frequency (ω) in rad/sec. The damping ratio (ξ) is then derived from the damping factor δ using relation 5.2

5.4.1 Mode 1

As highlighted in section 2.3 the aerodynamic instability can occur for a mode at any nodal diameter. Hence it is imperative to first find the nodal diameter giving the least aerodamping work and the corresponding damping ratio. The rotor disk under investigation has 37 rotor blades and thus 18 nodal diameters each in the backward and forward travelling wave pattern. The analysis is arbitrarily started at the 0 nodal diameter and continued for higher nodal diameters in the forward travelling direction. The results for the aerodamping work are plotted in figure 5.4.1 and for damping ratio in 5.4.2. All nodal diameters are not investigated in the current scope due to the large simulation times. The investigation is carried out for the first observed least stable nodal diameter.

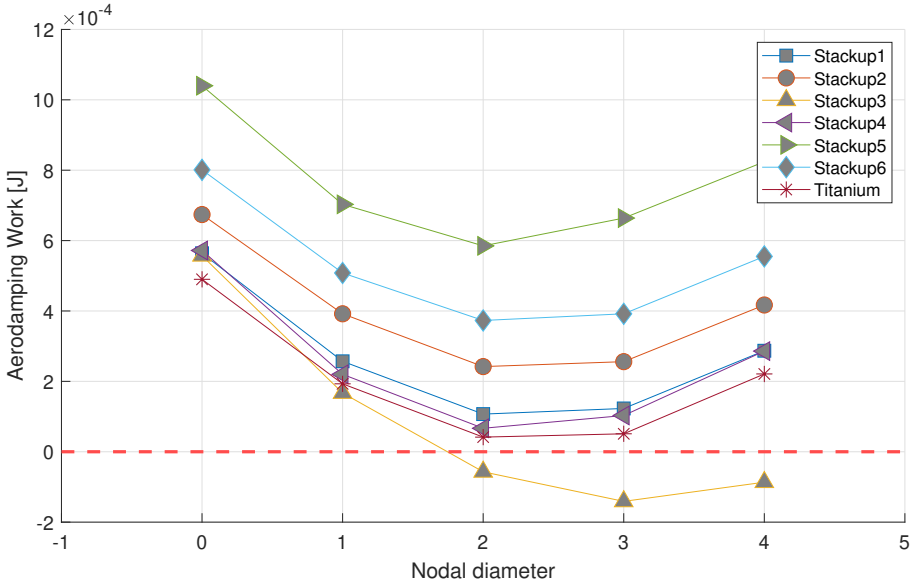

Figure 5.4.1: Aerodynamic damping work for the Mode 1 plotted against Nodal diameter

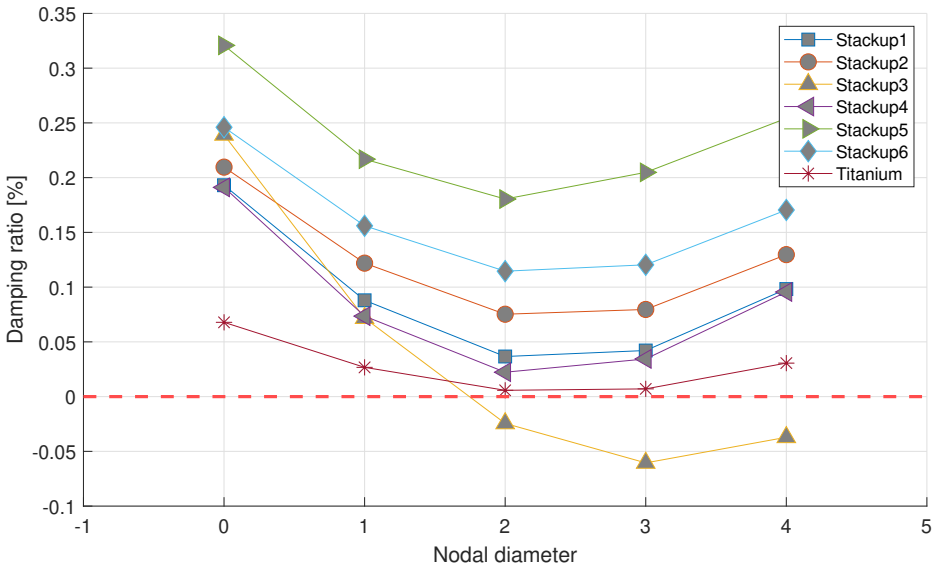

Figure 5.4.2: Aerodynamic damping ratio for the Mode 1 plotted against Nodal diameter

It is observed that Stackup 5 gives the highest aerodamping work which is 14 times the work of titanium blade and thus the most stability. Stackup 3 is the least stable stackup and has negative aerodamping for the nodal diameter 2 to 4 with the lowest damping for nodal diameter 3. All other stackups and the titanium blade exhibit the lowest damping for nodal diameter 2. Further investigation is made to establish the relation between the stackup, its vibration properties i.e modal shape and frequency, and the

aerodamping work. Nodal diameter 2 which shows the lowest damping for most of the stackups and the titanium blade is used for further investigations. The deflection of mode shape is observed as the twisting present at the tip of the blade. The information is extracted at the tip as shown in figure 5.4.3a. The twist for the investigated stackups can be visualised in figure 5.4.3b. It is to be noted that the deflections in the figure 5.4.3b are scaled down for better visualisation.

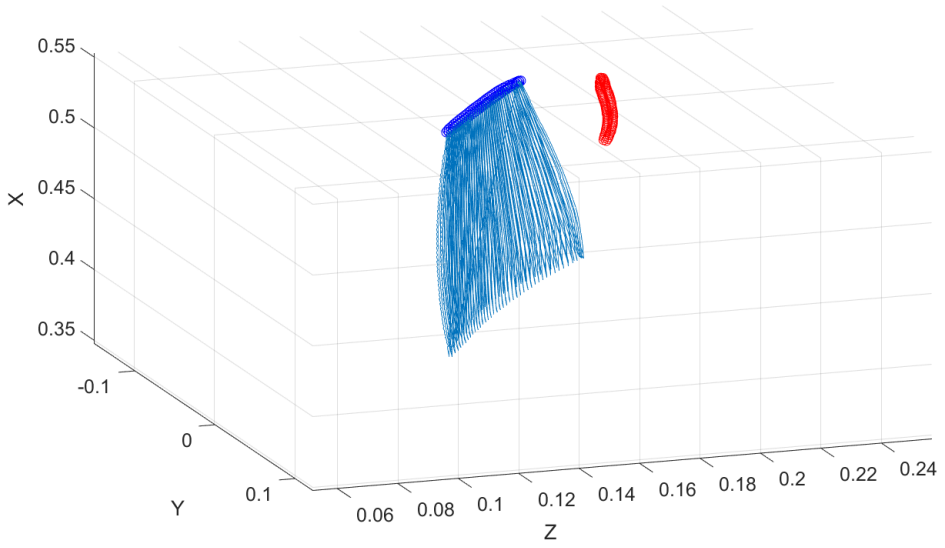

(a) Mode shape. Blue-original blade and blade tip, Red-Deflected blade tip

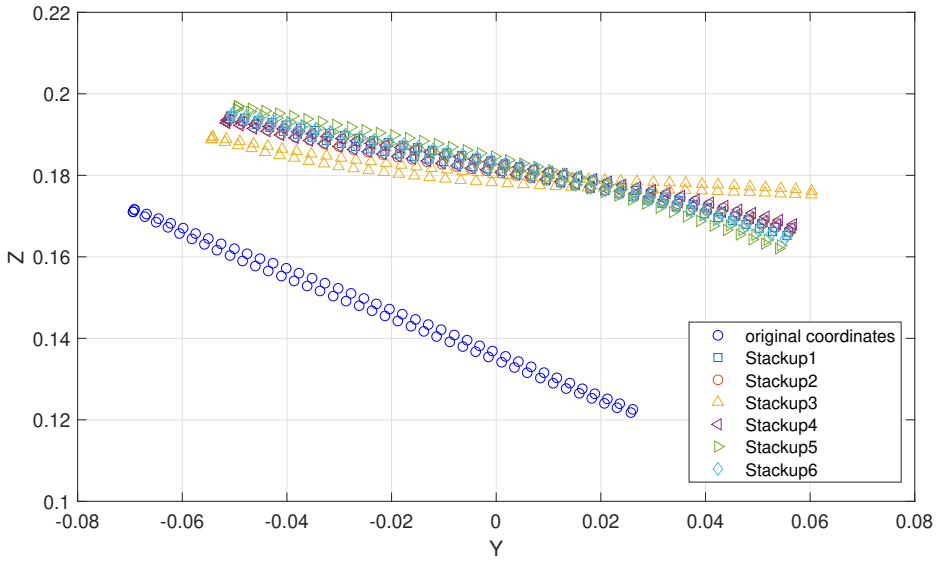

(b) Mode shape at the tip of blade

Figure 5.4.3: Mode shape of the blade and the twisting at the tip for the investigated stackups for Mode 1

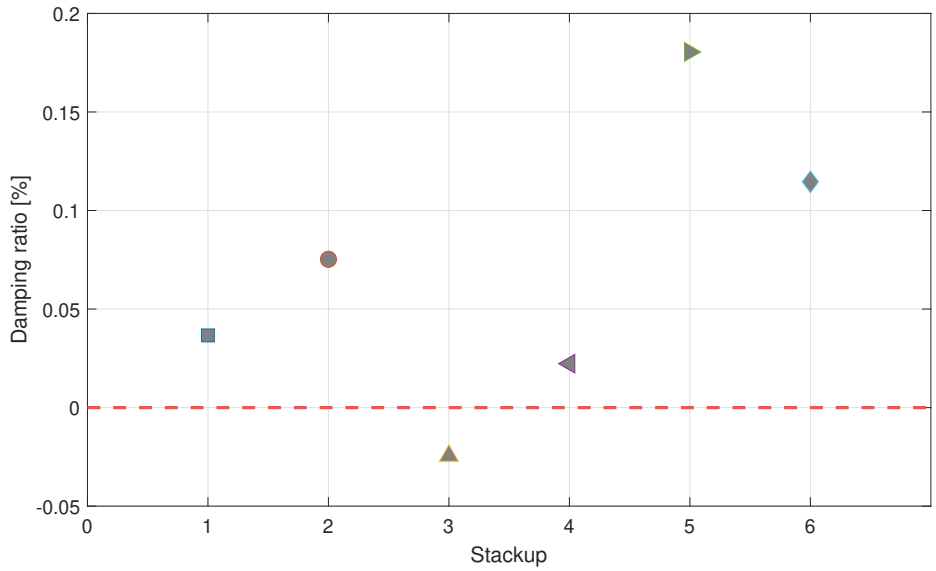

Figure 5.4.4: Aerodamping for the investigated stackups for the least stable Nodal diameter for Mode 1

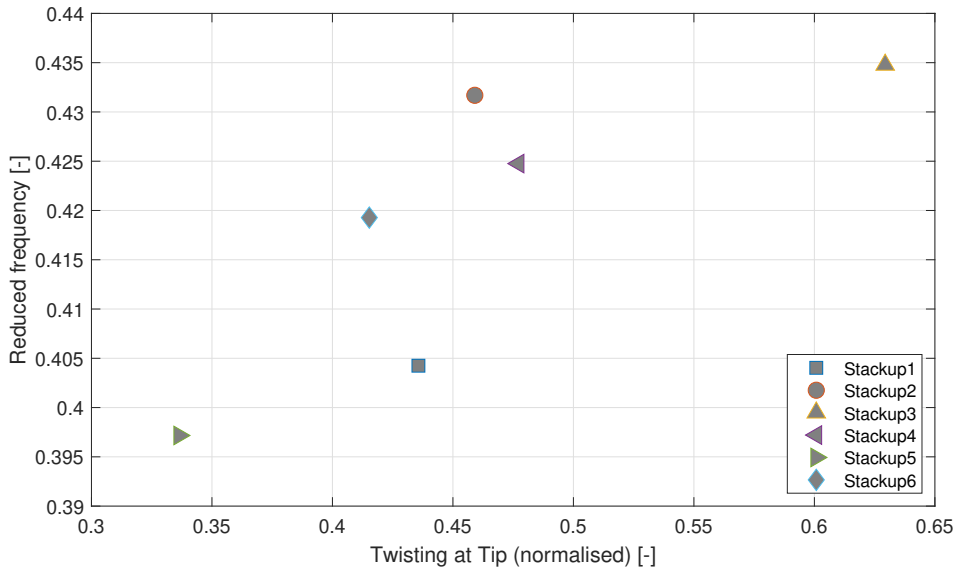

Figure 5.4.5: Values of reduced frequency and twisting at blade tip for Mode 1 for each stackup

For the least stable nodal diameter, the aerodamping ratio for each stackup is presented in figure 5.4.4 and the reduced frequency and twisting values for each stackup are presented in figure 5.4.5. Figure 5.4.5 is not to be interpreted as to have dependency between reduced frequency and twisting but it is done only to plot values in one graph. Stackup 3 with negative damping shows the highest twisting at the tip and highest reduced frequency while the most stable Stackup 5 has the lowest twisting and the

lowest reduced frequency. The twisting value is seen to dominate in these comparison where the higher twisting leads the Stackup 3 into unstable behaviour. Considering Stackup 6 and Stackup 1 or Stackup 2 and Stackup 4 in which the amount of twisting is relatively close the stackup with higher reduced frequency is observed to have a higher aerodamping ratio. Comparing Stackup 1 and Stackup 2, it is observed that Stackup 2 has a higher twisting and a higher reduced frequency. Here the higher reduced frequency dominates thus exhibiting a higher aerodamping ratio for Stackup 2. Thus it can be concluded that a combination of twisting and reduced frequency plays a role in the stability of the stackup. A lower twisting and higher reduced frequency is favourable for stability. For stackups with relatively similar amount of twisting the stackup with higher reduced frequency will tend to more stability.

Correlating the above results with the the ply angles in stackups it can be concluded that Stackup 5 with a configuration $[(45/45/0/-45/-45/0)_2/...]_s$ leads to lower twisting which is due to the higher shear stiffness provided by $\pm 45^\circ$ plies. Stackup 3 with configuration $[22.5/0/-22.5/-45/-22.5/0/22.5/45/0/-45/0/45/...]_s$ has some $\pm 45^\circ$ plies replaced with $\pm 22.5^\circ$ and also 22.5° plies positioned towards the outer surface. This leads to higher twisting and instability. Although the frequency is increased due to $\pm 22.5^\circ$ the high twisting results in negative damping. Stackup 2 $[(45/22.5/0/-22.5/-45)/0/(45/22.5/0/-22.5/-45)/-22.5/...]_s$ and Stackup 4 $[(45/0/-45/0)_3/...]_s$ have similar amount of twisting. Stackup 4 has twice the number of $\pm 45^\circ$ and no $\pm 22.5^\circ$ while Stackup 2 has 5 pairs of $\pm 22.5^\circ$ which contribute to an increase in longitudinal stiffness and thus increased frequency in Mode 1 leading to higher stability. Stackup 2 and Stackup 6 $[(45/45/22.5/0/-22.5/-45/-45)/0/(..)/-22.5/...]_s$ have equal number of plies for each angle in the overall stackup. The difference is in the arrangement where for Stackup 6, 45° plies are moved towards the outer surface thus resulting in higher shear stiffness, reduced twisting and reduced Mode 1 frequency. The reduction in twisting dominates and provides a higher damping.

Thus the number of plies of each angle and the arrangement of plies are both critical in influencing the reduced frequency and twisting. As most of the stackups here provide a positive damping it would be recommended to avoid more number of plies with lower angle on the outer side of the stackup to prevent large twisting and unstable behaviour. For increasing stability a good mix of $\pm 45^\circ$, $\pm 22.5^\circ$ and 0° plies is required with $\pm 45^\circ$ plies placed towards the outer surface to minimize deflection and the lower angles distributed so as to maximize frequency.

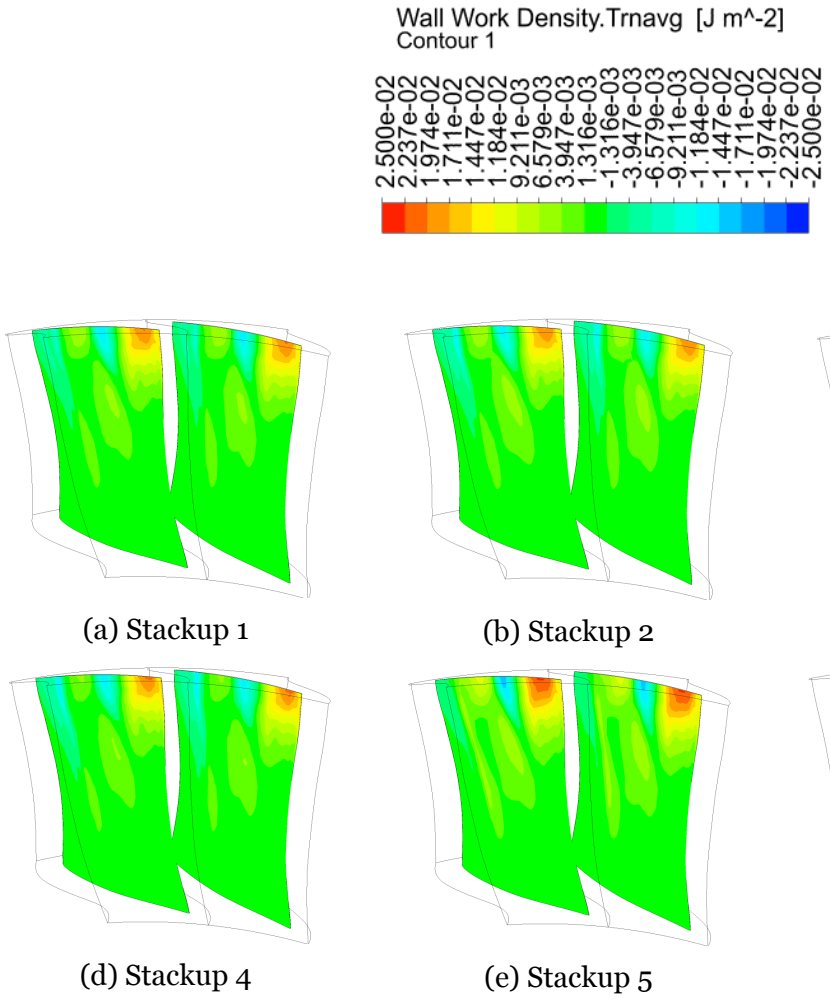

(a) Stackup 1 (b) Stackup 2 (c) Stackup 3

(d) Stackup 4 (e) Stackup 5 (f) Stackup 6

Figure 5.4.6: WWD trn avg on the suction side for 1st mode for Stackup 1 to 6

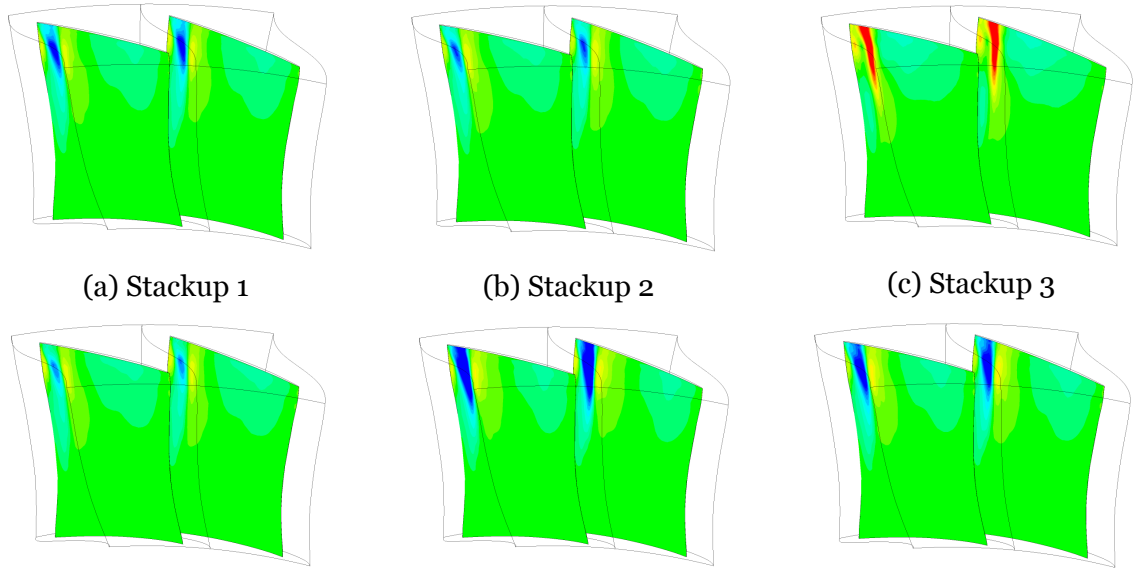

(a) Stackup 1 (b) Stackup 2 (c) Stackup 3

(d) Stackup 4 (e) Stackup 5 (f) Stackup 6

Figure 5.4.7: WWD trn avg on the Pressure side for 1st mode for Stackup 1 to 6

It is further of interest to look at the qualitative distribution of the work over the blade. Hence the contours of Wall work Density transient average over period are plotted and represented in figure 5.4.6 for the suction side and figure 5.4.7 for the pressure side. The legend common to the figures is plotted above the figures.

From the figures it can be observed that the negative wall work density values, i.e destabilising behaviour are towards the tip of the blade. The maximum of the positive and negative wall work density are located near the leading edge tip. On the suction surface the stable Stackup 5 has higher values of positive wall work on the leading edge tip while the unstable Stackup 3 has relatively smaller values. Stackup 3 also shows a dominant negative wall work towards the trailing edge of the blade. On the pressure side the stable Stackup 5 shows a dominant negative region towards the leading edge tip. However moving towards the trailing edge the values appear to be positive. Stackup 3 in contrast shows a dominant positive region on the leading edge tip and negative values as one moves towards the trailing edge. Further to look into quantitative data the spanwise distribution of Wall work density is calculated and plotted in figure 5.4.8 for Stackup 3 and Stackup 5. The blade is divided into 99 spanwise cuts and the Wall work density is integrated over the length of the span circumference.

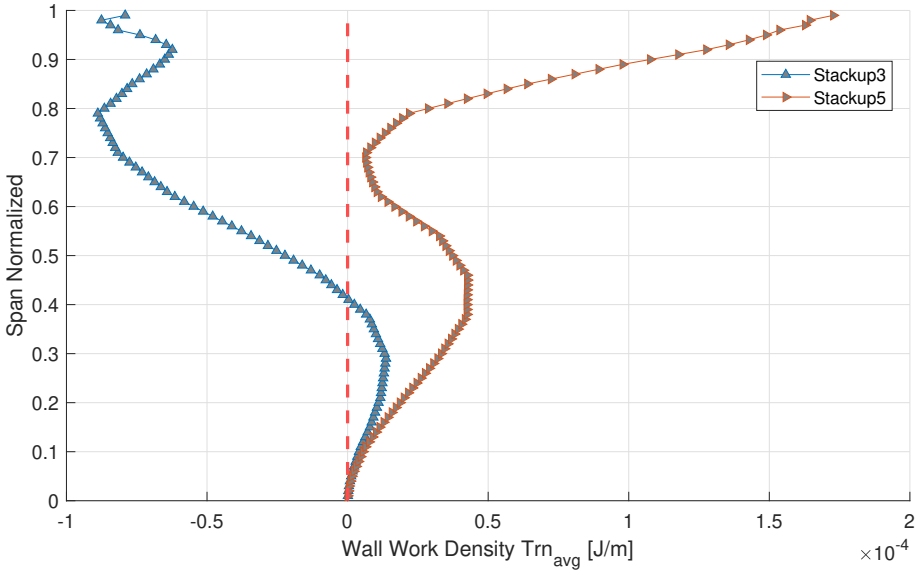

Figure 5.4.8: Wall work density distribution along the span direction for the most stable Stackup 5 and least stable Stackup 3 for Mode 1

It can be observed that Stackup 3 shows a negative work density on most span of the

blade with a positive work on 40 % span of blade from the hub. The negative values increase considerably beyond 50 % span. Stackup 5 has a positive work density on the complete span. The region above 80% span to the tip is seen to have a bigger contribution for Stackup 5.

5.4.2 Mode 2

As for Mode 1 the analysis for Mode 2 is started at nodal diameter 0 and continued for higher nodal diameters in the forward travelling direction. The figure 5.4.9 shows the aerodamping work values and the figure 5.4.10 shows the corresponding damping ratio.

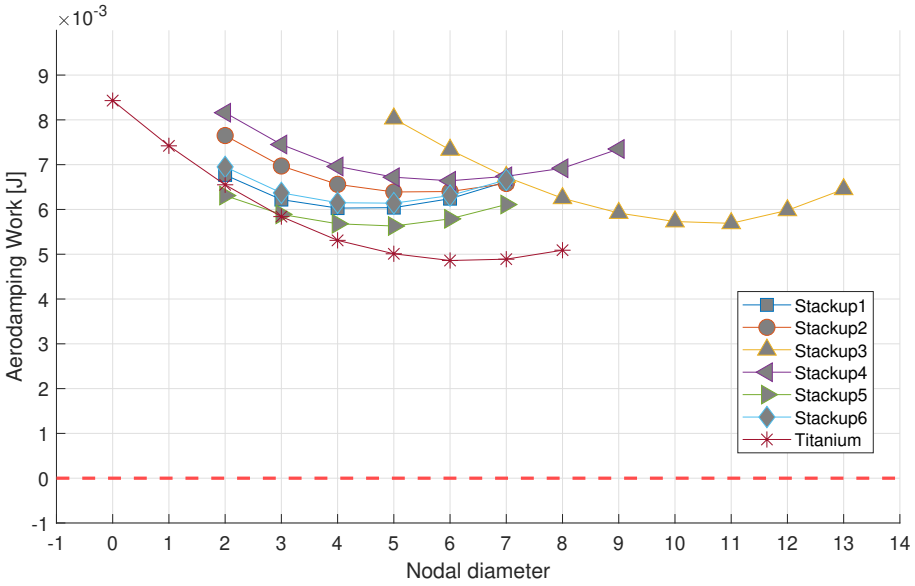

Figure 5.4.9: Aerodynamic damping work for the Mode 2 plotted against Nodal diameter

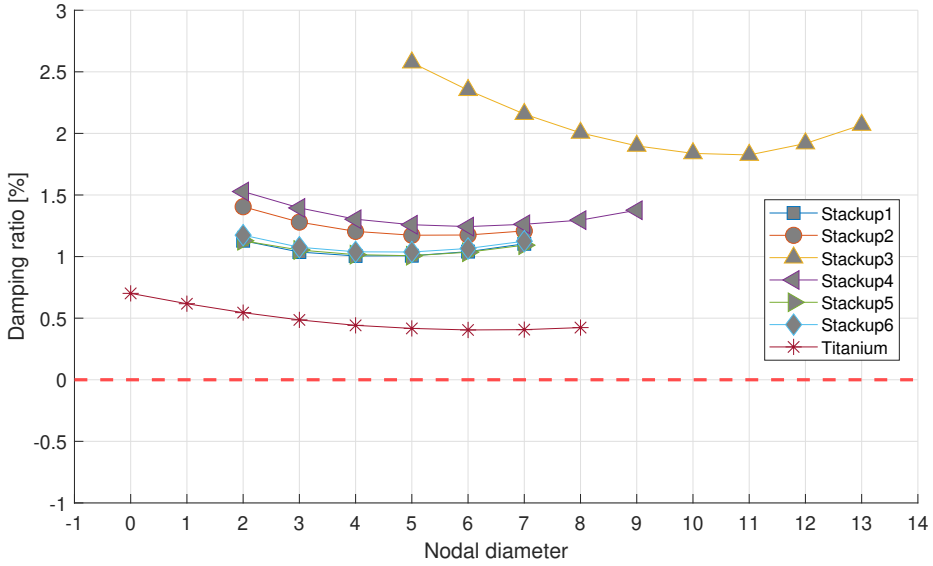

Figure 5.4.10: Aerodynamic damping ratio for the Mode 2 plotted against Nodal diameter

The values are plotted for nodal diameter 0 to 8 for the titanium blade which is observed to have lowest values for work and damping ratio at nodal diameter 6. All stackups are found to have a positive damping and also damping higher than the titanium blade. All composite stackups, except for Stackup 3, show a minimum value of work and damping ratio for nodal diameter 5 or 6. Stackup 3 shows a minimum value for nodal diameter 11 and the curve of work and damping ratio can be observed to have a shift compared to other stackups. To investigate this effect, the mode shape of the blade are observed at the tip as shown in figure 5.4.11a

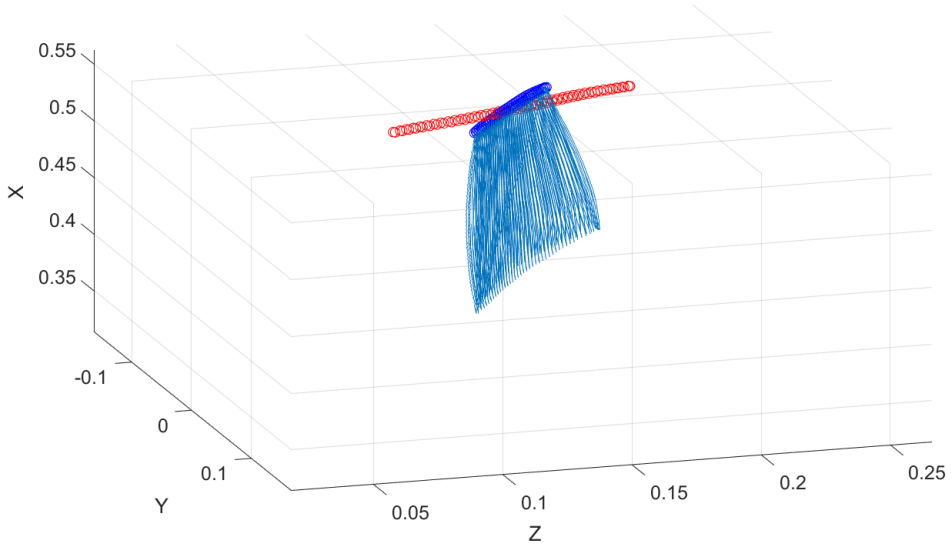

(a) Mode shape. Blue-original blade and blade tip, Red-Deflected blade tip

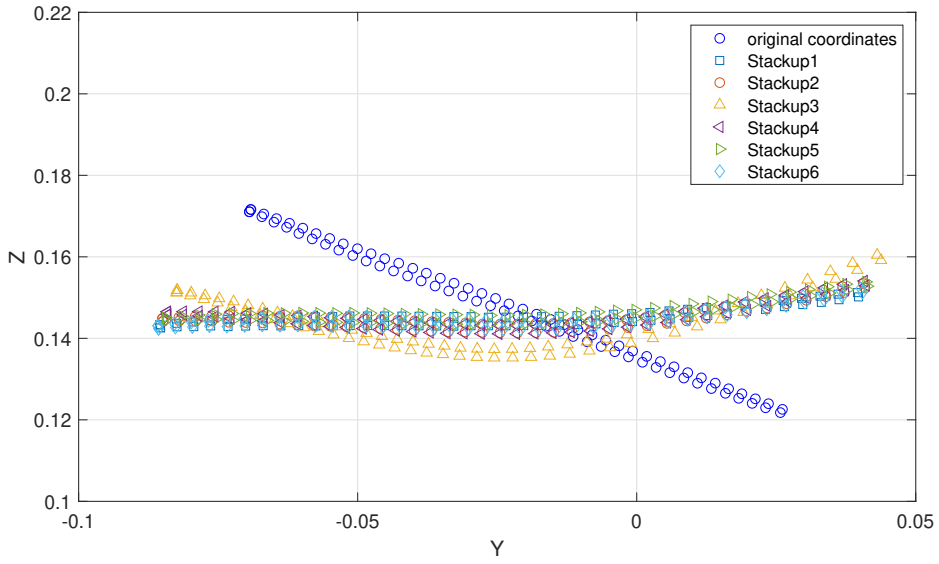

(b) Mode shape at the tip of blade

Figure 5.4.11: Mode shape of the blade and the twisting at the tip for the investigated stackups for Mode 2

Qualitatively observing the deflection of tip, it is observed that Stackup 3 has the inflection point moved towards the leading edge (right) of the blade. Also the trailing edge (left) of the blade is less deflected and the mode shape is seen to bulge after the inflection point towards the trailing edge thus deviating the mode shape from conventional torsional behaviour. This can be seen as a result of having 22.5° plies on the outer surface of the stackup. This leads to lower tip to tip twisting of the blade which can be seen in figure 5.4.11b.

From figure 5.4.13 and 5.4.12, Stackup 3 having 22.5° plies on the outer surface has the highest damping ratio and lowest twisting. This is followed by Stackup 4 which has a higher number of 0° towards the outer surface and shows the second highest value for damping ratio and second lowest value for twisting. Stackup 5 with higher number of ±45° plies towards the outer surface exhibits the lowest damping ratio and has a intermediate value of twisting and highest value of reduced frequency. The damping ratio values for stackups other than Stackup 3 are quite close and strong relation between reduced frequency and twisting cannot be stated here. It can only be concluded that using lower value of ply angle towards the outer plies in the stackup lead to stable behaviour in Mode 2.

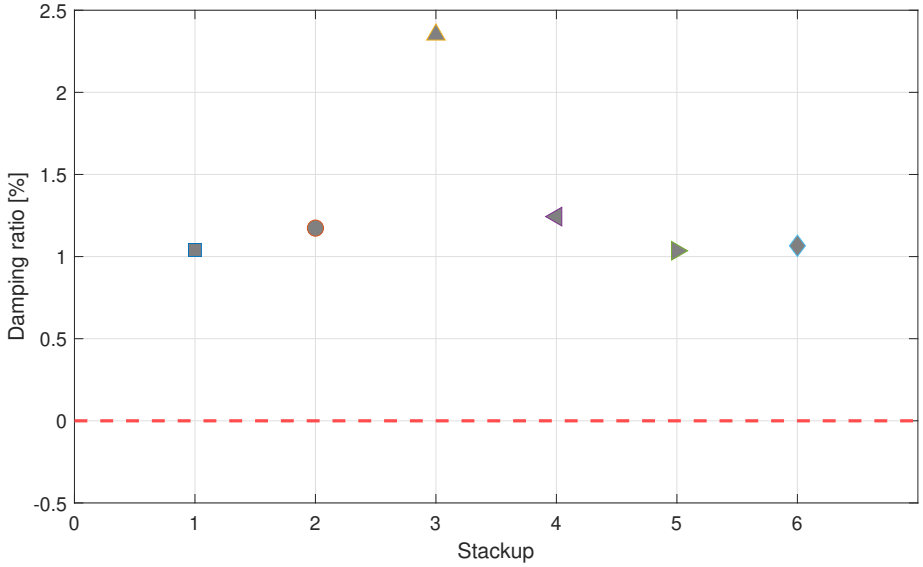

Figure 5.4.12: Aerodamping for the investigated stackups for the least stable Nodal diameter for Mode 2

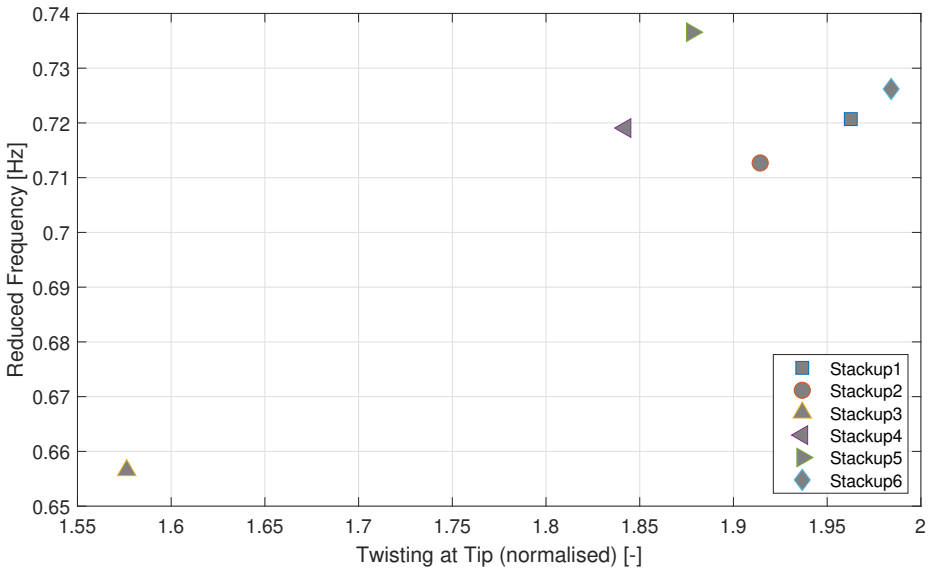

Figure 5.4.13: Values of reduced frequency and twisting at blade tip for Mode 2 for each stackup

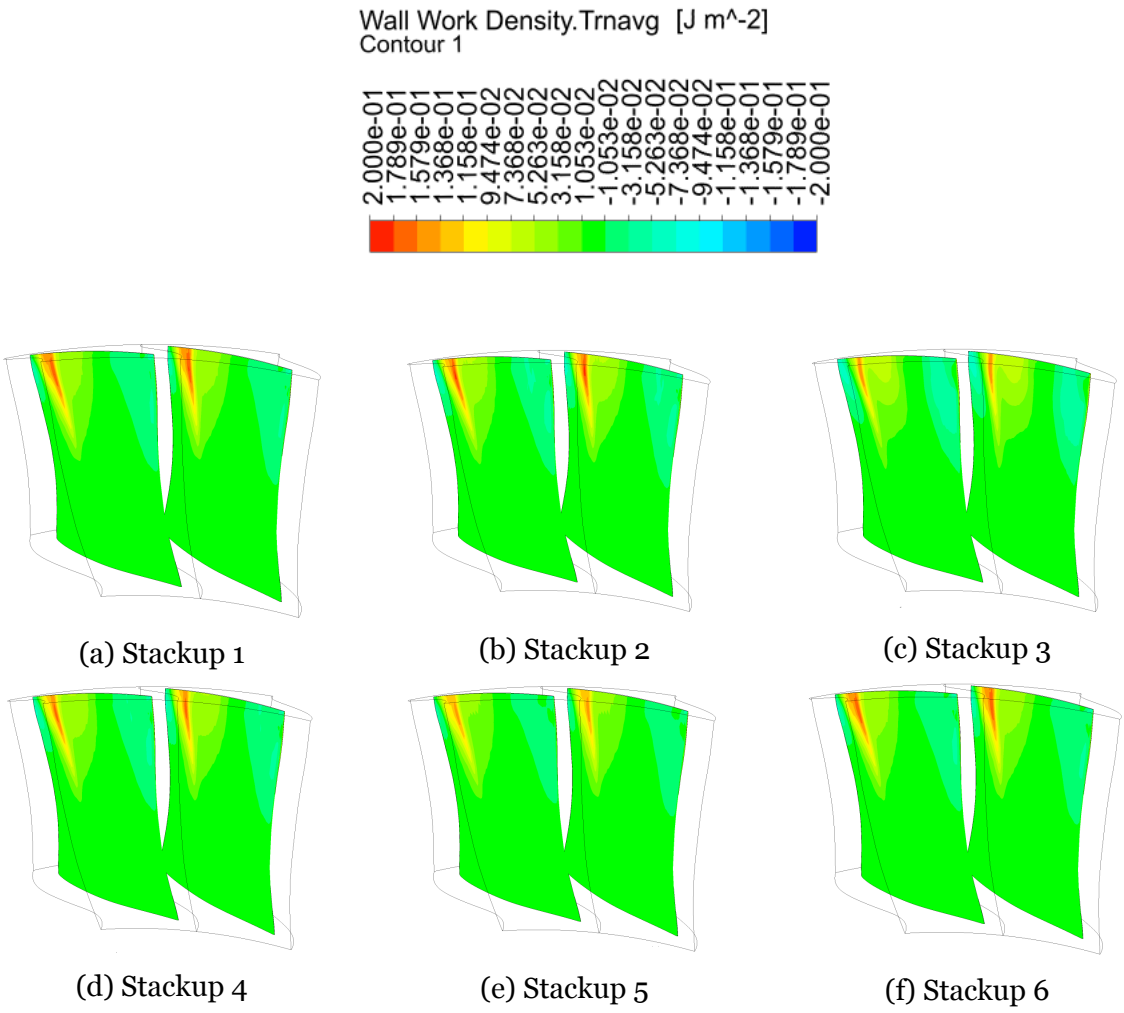

(a) Stackup 1 (b) Stackup 2 (c) Stackup 3

(d) Stackup 4 (e) Stackup 5 (f) Stackup 6

Figure 5.4.14: WWD trn avg on the suction side for 2nd mode for Stackup 1 to 6

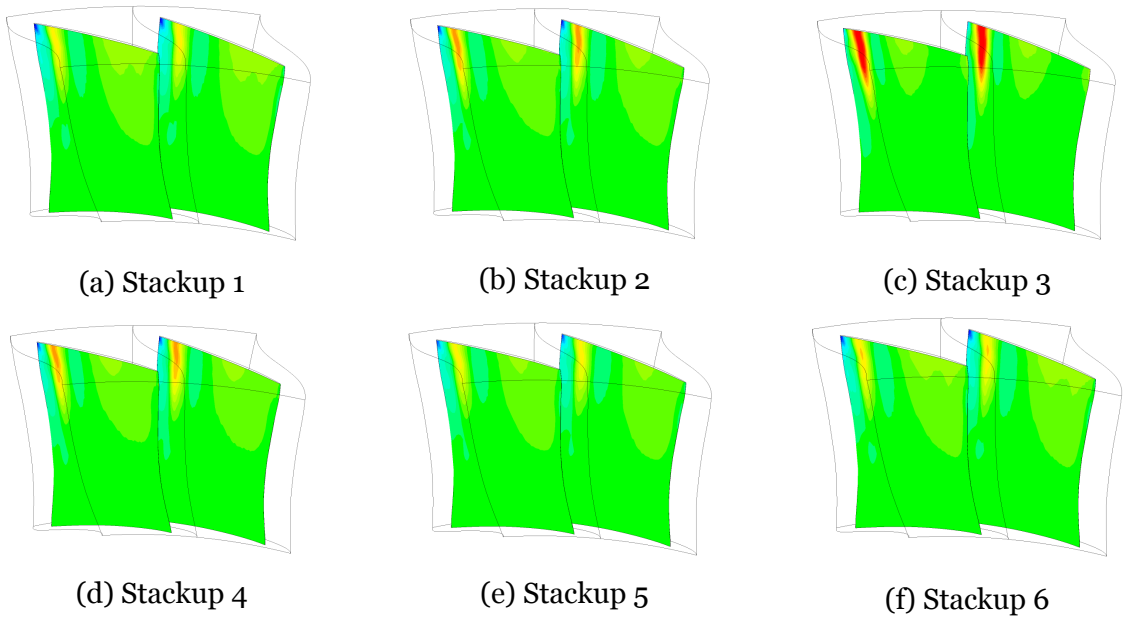

(a) Stackup 1 (b) Stackup 2 (c) Stackup 3

(d) Stackup 4 (e) Stackup 5 (f) Stackup 6

Figure 5.4.15: WWD trn avg on the pressure side for 2nd mode for Stackup 1 to 6

The contours for Wall work density in figures 5.4.14 and 5.4.15 show a maximum of work towards the trailing edge on the suction side and towards the leading edge on the pressure side. The most stable stackup, Stackup 3 shows a dominant positive wall work on the pressure side as compared to other stackups.

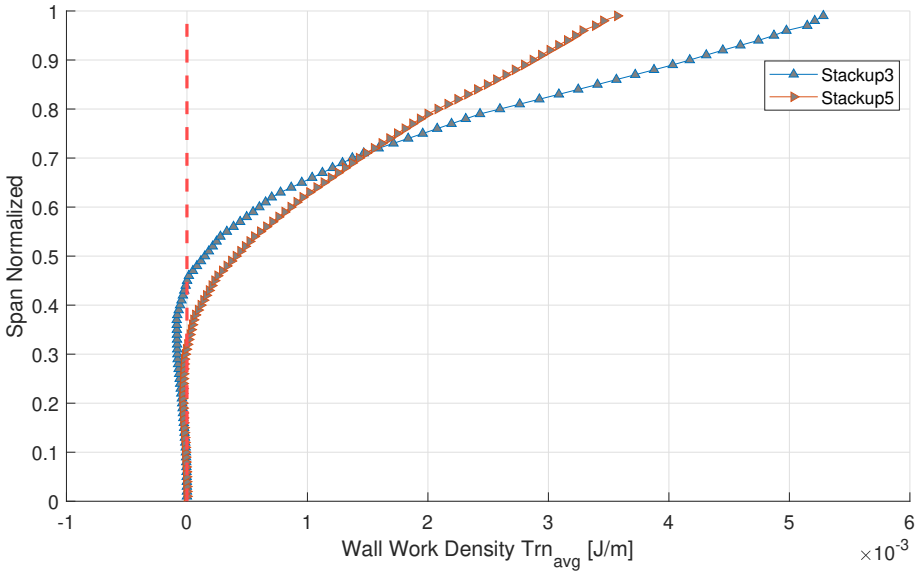

Figure 5.4.16: Wall work density distribution along the span direction for the most stable Stackup 5 and least stable Stackup 3 for Mode 2

The distribution of Wall work density along the span in figure 5.4.16 shows a change beyond 50% span. The change increases significantly beyond 70% span.

Chapter 6

Conclusions

The objectives to built a composite blade in Ansys ACP, investigating flutter stability and establishing the relation between ply angle configurations in stackup and stability were achieved. The anisotropic properties of composites are found to have a potential in tailoring the vibration behaviour just by changing the angles in the ply stackup and have a stabilising or destabilising effect on the flutter behaviour. A methodology to build the composite model was established which once created gave a easy approach to modification of stackup angles and ply lengths using the built-in excel interface.

Six different ply stackup configurations were investigated in the scope of project with a combinations of $\pm 60^{\circ}$, $\pm 45^{\circ}$, $\pm 22.5^{\circ}$ and 0° plies. The modal analysis results for Mode 1, indicated a decrease in shear stiffness and a higher twisting in the mode shape for a stackup with higher number of $\pm 22.55^{\circ}$ and 0° plies and arrangement of those plies on outer surface. For Mode 1, the lowest twisting was exhibited by stackups with higher number of $\pm 45^{\circ}$ and arrangement on outer surface. For Mode 2, lower ply angles affected the mode shape in way to deviate it from the classical torsion behaviour and were observed to have lower twisting at tip in the mode shape. For stackups with same number of plies of particular angle the twisting and stiffness showed a dependency on the the arrangement of plies. The frequencies for Mode 1 were observed to be higher with stackups having higher number of lower angle plies and thus higher longitudinal stiffness. For Mode 2, stackups with higher number of $\pm 45^{\circ}$ resulted in higher shear stiffness and higher frequencies.

The aerodamping analysis for Mode 1 indicated a higher stability for Stackups with 45° plies placed on the outer surface. The only unstable stackup was with higher number

of $\pm 22.5^\circ$ towards the outer surface. Overall a lower twisting at the tip and higher reduced frequency was found favourable for flutter stability in Mode 1. For Mode 2 a contradictory effect was observed where the plies with lower angle were found to change the mode shape in a way to reduce the twisting at the tip. This led to the least stable stackup for Mode 1 with 22.5° ply towards the outer surface to have the highest stability for Mode 2. Thus a stackup with stabilising behaviour in one mode could have a destabilising effect for the other mode.

It could be of interest to check all the nodal diameters for stability which was not feasible in the time constraints of the current project. It could also be of interest to investigate more ply angles like $\pm 15^\circ$ and $\pm 30^\circ$ to study their relative effects. Finally, an experimental validation would be of greater interest to establish a process starting from numerical analysis to final working prototype.

Bibliography

[1] "Aeromechanics Course Notes, KTH". In: *KTH, HPT Lab* (2020).

[2] Ahmed, Junaid Kameran. "Parametric Study on Dynamic Analysis of Composite Laminated Plate". In: *International Journal of Civil and Environmental Engineering,World Academy of Science* (2017).

[3] Ansys. "Ansys User guides". In: *Ansys Help documentation* (2019 R3).

[4] AV Srinivasan DG Cutts, S Sridhar. "Turbojet engine blade damping". In: (1981).

[5] B.Brouillet. "Zeitgenaue dreidimensionale Simulation des Flatterns in Turbomaschinen durch numerische L¨osung der Navier-Stokes-Gleichungen". In: *Ph.D. Thesis, Technical University of Aachen* (2001).

[6] Bendiksen, O. O. "Recent Developments in Flutter Suppression Techniques for Turbomachinery Rotors". In: *J. PROPULSION* (1987). DOI: 10.2514/3.51283.

[7] Brian L. Kemp, Eric R. Johnson. "Response and failure analysis of a graphite-epoxy laminate containing terminating internal plies". In: *American Institute if Aeronautics and Astronautics* (1985).

[8] Bruyneel, Michaël. "A course on Mechanics of Composites". In: *University of Liege* (2020-2021).

[9] C. Reiber, M. Blocher. "Potential of Aeroelastic Tailoring to Improve Flutter Stability of Turbomachinery Compressor Blades". In: *ASME Turbo Expo 2017* (2017). DOI: ETC2017-180.

[10] Ceyhun Tola, Altan Kayran. "The effect of fiber orientation angle and ply thickness on subsonic and supersonic flutter characteristics of a composite missile fin". In: *Ankara International Aerospace conference* (2013). DOI: AIAC-2013-112.

[11] Collar, A. R. “The expanding domain of aeroelasticity”. In: *The Royal Aeronautical Society* (1946).

[12] Jao-Hwa Kuang, Ming-Hung Hsu. “The effect of fiber angle on the natural frequencies of orthotropic composite pre-twisted blades”. In: *Composite Structures,Science Direct* (2002). DOI: 10.1016/S0263-8223(02)00135-6. URL: https://doi.org/10.1016/S0263-8223(02)00135-6.

[13] Jiaguangyi Xiao Yong Chen, Qichen Zhu. “A general ply design for aero engine fan blade components”. In: *ASME Turbo Expo 2017* (2017). DOI: GT2017-64377.

[14] Kellner, Tomas. “https://www.ge.com/news/reports/the-art-of-engineering-the-worlds-largest-jet-engine-shows-off-composite-curves”. In: *GE* (2016).

[15] Lane, Frank. “System mode shapes in the flutter of compressor blade rows”. In: *Journal of the Aeronautical Sciences 23.1* (1956).

[16] Mehmed, O. “ Experimental classical flutter results of a composite advanced turboprop model”. In: *NASA Technical memorandum* (1986). DOI: NASA-TM-8879219860019799.

[17] Montgomery.et.al, Matthew. “Application of Unsteady Aerodynamics and Aeroelasticity in Heavy-Duty Gas Turbines”. In: *ASME Turbo Expo 2005: Power for Land, Sea, and Air. American Society of Mechanical Engineers. 2005, pp. 635–649.* (2005).

[18] N. Forsthofer, C. Reiber. “Structural mechanic and aeroelastic approach for design and optimization of CFRP blades”. In: ().

[19] T. Wollmann N. Modler, M. Dannemann. “Design and testing of composite compressor blades with focus on the vibration behaviour”. In: *Composites: Part A, Science Direct* (2017). DOI: 10.1016/j.compositesa.2016.06.012.

[20] Vogt, Damian. “Lecture Notes MJ2430 / MJ2244, KTH”. In: *KTH, HPT Lab* (2009).

Appendix Contents

Appendix A

Ansys APDL Command file to extract mode shapes

```
/post1
NDs=9 !ND+1
num_mode=6

!!The modes that are exported with this option are normalized by the max
displacement of each mode
exun,surf,disp,comm,si  !!Calls the EXUNIT APDL command
*do,jd,1,NDs,1
*do,jm,1,num_mode,1
alls
set,jd,jm,,REAL
cmsel,,Blade_PS
cmsel,a,Blade_SS
cm,BladeSurf,elem
jdp=jd-1
expr,surf,mode,,BladeSurf,BladeSurfNorm_ND%jdp%_M%jm%,csv, !!Calls the
EXPROFILE APDL command
expr,surf,disp,,BladeSurf,BladeSurf_ND%jdp%_M%jm%,csv, !!Calls the
EXPROFILE APDL command
*enddo
*enddo
alls
/post1
/output,'frequencies',txt
set,list
/output
```